Doctoral Thesis

Electrochemical Properties of Vanadium Hydride for All-Solid-State Lithium-Ion-Batteries

Yasuhiro Matsumura

Graduate School of Integrated Arts and Sciences
Hiroshima University

March 2020

Doctoral Thesis

Electrochemical Properties of Vanadium Hydride for All-Solid-State Lithium-Ion-Batteries

Yasuhiro Matsumura

Division of Integrated Arts and Sciences
Graduate School of Integrated Arts and Sciences
Hiroshima University

March 2020

1. Thesis Title

Electrochemical Properties of Vanadium Hydride for All-Solid State Lithium Ion Batteries

(全固体リチウムイオン電池における水素化バナジウムの電気化学特性)

Yasuhiro Matsumura

2. Research article

(1) Vanadium Hydride as Conversion Type Negative Electrode for All-Solid-State Lithium-ion-battery

Yasuhiro Matsumura, Keiji Takagishi, Hiroki Miyaoka and Takayuki Ichikawa

Materials Transactions, 60, 2183-2187 (2019).

Contents

1. Introduction

1.1 Long term prospects of electricity demand

In 2015, COP 21 (United Nations Framework Convention on Climate Change 21st Conference of the Parties) was held in Paris, France. The content of this Paris Agreement is to promote the reduction of global average temperature rise to less than 2 degrees (mentioning that keeping at 1.5 degrees to greatly contribute to risk reduction) in the whole world in the second half of this century, we have set out a direction to substantially reduce greenhouse gas emissions by human activities [1-1, 1-2].

Targets have been set in Japan, and various policies are beginning to be considered. In Japan, the goal is to reduce greenhouse gas emissions in 2030 by 26% from the level in 2013 as a medium-term goal [1-3]. The first core for achieving these goals is to promote low-emission long-term energy supply and demand prospects (energy mix) by increasing the amount of renewable energy (solar, wind, tidal, biomass, sea waves and so on) to be introduced, and to pursue further energy efficiency. In the energy mix of 2030 shown by the Japanese government, the prospects of the power supply composition such as renewable energy 22 to 24% and nuclear power 22 to 20% are shown together with thorough energy saving. The renewable energy such as solar power and wind power

generation has a weak point that the amount of power generation is influenced by the weather and it is hardly controlled. Thus, the renewable energy trends to be over or under supplied to demand. There is no mechanism to balance supply and demand because there is no adjustment in the renewable energy itself. As a result, there is a risk of large-scale power outages. If surplus electricity can be stored, it will be easier to balance supply and demand. And it can also be used as an adjustment force when there is not enough. Therefore energy storage and secondary batteries are expected as solutions for stably supplying such energy.

1.2 Power storage system

Currently, there is a wide variety of accumulators, which are roughly classified into chemical cells that generate electricity through internal chemical reactions and take out their energy, and physical cells that convert physical energy such as solar cells into electric energy. In addition, chemical batteries are divided into two battery types. One is primary batteries that are used up. Another is secondary batteries that can be used repeatedly by charging them. This secondary battery is expected for stable supply of renewable energy.

There are also various types of secondary batteries. (a) Lead-acid battery, (b) Sodium-sulfur battery (NAS battery), (c) Nickel metal-hydride battery, (d) Lithium-ion-battery. A brief explanation will be given for each battery.

1.2.1 Lead-acid battery

Lead-acid batteries consist of lead dioxide as the positive electrode, metallic lead as the negative electrode, and dilute sulfuric acid as the electrolyte. Electrical energy is extracted by causing the following chemical reaction. In the reaction of both electrodes, each electrode active material and sulfate ions in the electrolytic solution are consumed to produce lead sulfate.

Positive electrode: $PbO_2 + 4H^+ + SO_4^{2-} + 2e^- \leftrightarrow PbSO_4 + 2H_2O$ (1-1)

Negative electrode: $Pb + SO_4^{2-} \leftrightarrow PbSO_4 + 2e^-$ (1-2)

Whole reaction: $PbO_2 + Pb + 2H_2SO_4 \leftrightarrow 2PbSO_4 + 2H_2O$ (1-3)

The average operating voltage of the lead acid battery is 2.041 **V**, the gravimetric energy density is 20-35 Wh/kg, and the volumetric energy density is 50-90 Wh/L [1-4]. Since it is low cost, it is widely applied to automobiles. However, since lead is used for the electrode material, the weight becomes large and the energy density can't be increased.

1.2.2 Sodium-sulfur battery (NAS battery)

As a large power storage system, Sodium-sulfer batteries have already been used for demonstration experiments. This battery is called NAS battery. In this NAS battery, sodium (Na) and sulfur (S) are used as a negative electrode and positive electrode respectively. $\beta-Al_2O_3$ based on ionic conductor for Na ion is used as a solid electrolyte, causing a chemical reaction between sulfur and sodium ions [1-5].

Positive electrode: $xS + 2Na^+ + 2e^- \leftrightarrow Na_2S_x$ (1-4)

Negative electrode: $2Na \leftrightarrow 2Na^+ + 2e^-$ (1-5)

Whole reaction: $2Na + xS \leftrightarrow Na_2S_x$ (1-6)

The operating voltage of the NAS battery is in the range of 1.78–2.076 **V** at 350 °C and the gravimetric energy density is 100-200 Wh/kg [1-6]. It is characterized by its high energy density and rate characteristics, allowing rapid charging and discharging. However, in order to increase the ionic conductivity of the solid electrolyte, high temperature operation at about 300 °C is necessary.

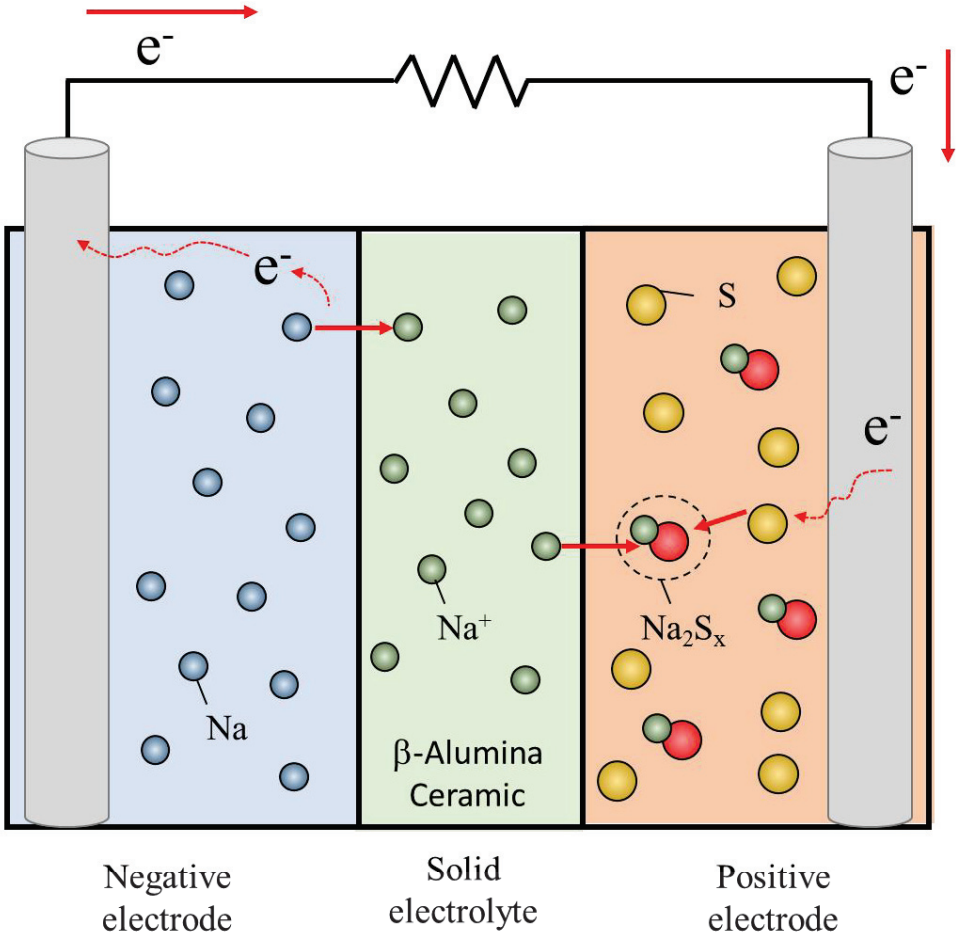

Figure 1-1 Schematic diagram of operating principle for NAS batteries [1-7]. The blue spheres represent the sodium atom and the green spheres represent the sodium ion. The yellow spheres indicate the sulfur atom. In the discharging process, sodium ions move through the ceramic electrolyte and react with sulfur atoms.

1.2.3 Nickel metal-hydride battery

Nickel metal hydride battery has a structure in which nickel oxyhydroxide (β-NiOOH) is used as a positive electrode, a metal hydride capable of atomic hydrogen can enter and leave a negative electrode, and potassium hydroxide is used as an electrolytic solution [1-8]. The chemical reactions occurring at both electrodes are as follows.

Positive electrode: $NiOOH + H_2O + e^- \leftrightarrow Ni(OH)_2 + OH^-$ (1-7)

Negative electrode: $MH_x + OH^- \leftrightarrow M + H_2O + e^-$ (1-8)

M = Metal elements

Whole reaction: $NiOOH + MH_x \leftrightarrow Ni(OH)_2 + M$ (1-9)

Electrons move from the side of the metal hydride where electron energy is high, and the nickel oxyhydroxide of the positive electrode reacts with water in the electrolytic solution and is reduced to $Ni(OH)_2$. The operating voltage of the nickel metal hydride battery is 1.2 **V**, the gravimetric energy density is 60-120 Wh/kg, and the volumetric energy density is 140-300 Wh/L. Nickel metal hydride batteries have high energy density and high cycle characteristics. Then, there is less danger of ignition and safety is high.

1.2.4 Lithium-ion-batteries

Lithium-ion-batteries are composed of lithium metal oxides such as cobalt (Co) and manganese (Mg) as a positive electrode, graphite or lithium titanate as a negative electrode, electrolyte mixed with ethylene carbonate (EC) or dimethyl carbonate (DMC) as a solvent, and $LiPF_6$ such as a Li salt . The reaction formula of the lithium-ion-battery in the case of using lithium metal oxide as the positive electrode active material and graphite as the negative electrode active material is shown below

Positive electrode: $Li_{(1-x)}MO_2 + xLi^+ + xe^- \leftrightarrow LiMO_2$ (1-10)

M = Metal elements（for example: Ni, Mn, Co）

Negative electrode: $Li_xC \leftrightarrow C + xLi^+ + xe^-$ (1-11)

That is, as the whole battery,

$$Li_{(1-x)}MO_2 + Li_xC \leftrightarrow LiMO_2 + C \quad (1\text{-}12)$$

Compared with the other secondary batteries, lithium-ion-batteries have a very large energy density. It can operate at high voltage of 3-4 **V**. The advantage of lithium-ion-

batteries is that the energy density is high as shown in Figure 1-2. Compared with the other secondary batteries such as nickel cadmium and nickel metal hydride batteries, the volume and weight give double and triple energy densities. It is compact and lightweight, making it ideal for powering portable electronic equipment.

Next, in the case of lithium-ion-batteries, the high voltage is obtained. Approximately triple the voltage is obtained compared with nickel cadmium or nickel metal hydride batteries. In other words, to obtain the same voltage is to use only one third of the number of batteries. Because lithium-ion-batteries have higher energy density than the other secondary batteries, it can be said that secondary batteries are inherently a safety issue.

Currently, organic solvents as electrolytes are used in the commercially available lithium-ion-batteries, so there is a danger of ignition at high temperatures, which may cause overheating or even overdischarge. Due to the high energy density, many accidents have occurred because of short-circuiting and overheating in recent years, which causes the batteries to inflate extremely and ignite.

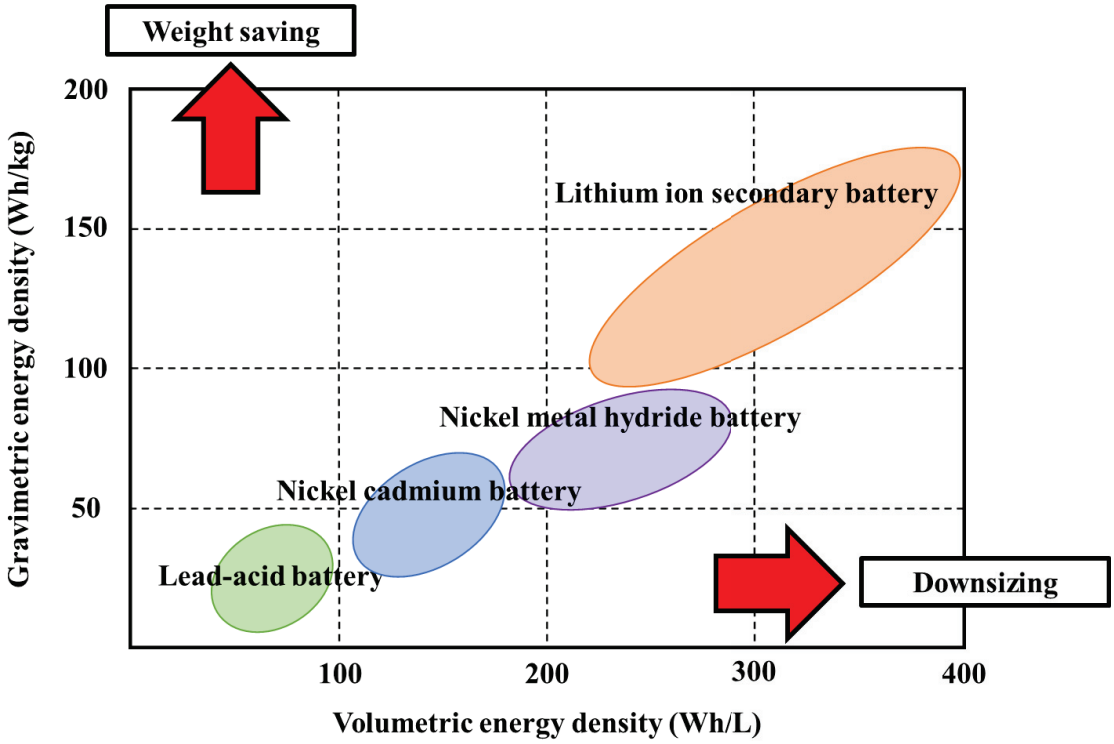

Figure 1-2 Energy density comparison of secondary batteries [1-9]. The horizontal axis shows the volumetric energy density. The vertical axis shows the gravimetric energy density. The higher the volumetric energy density, the smaller the battery. The higher the energy density by weight, the lighter the battery.

1.3 Principle of lithium-ion-battery

Charging and discharging are carried out by lithium ions moving between the positive electrode and the negative electrode through the electrolyte solution inside the lithium-ion-battery. Lithium ion enters the gap between the layers of the positive electrode material and the negative electrode material, and a chemical reaction occurs on each electrode.

For example, lithium ions are extracted from the interlayer of $LiCoO_2$ of the positive electrode material by charging and inserted into the graphite layer of the negative electrode (Figure 1-3). Conversely, at the time of discharge, lithium ions are released from the graphite layer of the negative electrode material and taken into the oxide of the positive electrode (Figure 1-4). The reaction caused by charging and discharging is basically only the movement of lithium ions. In the case of a lead-acid battery which is a conventional battery, SO_4^{2-} ions dissolve out at both the positive electrode and the negative electrode at the time of discharge, and as the discharge continues, the concentration of the SO_4^{2-} ion in the electrolytic solution gradually increases. At the time of charging, the concentration of SO_4^{2-} ion decreases. In this way, in the case of the lead-acid battery, there is a change in the concentration of the electrolytic solution due to

charging and discharging. However, in the case of a lithium-ion-battery, since lithium ions move only, the lithium ion concentration in the electrolytic solution does not change due to charging and discharging. Moreover, in the case of a lithium-ion-battery, the operating voltage, capacity and safety vary greatly depending on what is used for the positive electrode, the negative electrode, and the electrolytic solution. The roles and features of each component will be described below.

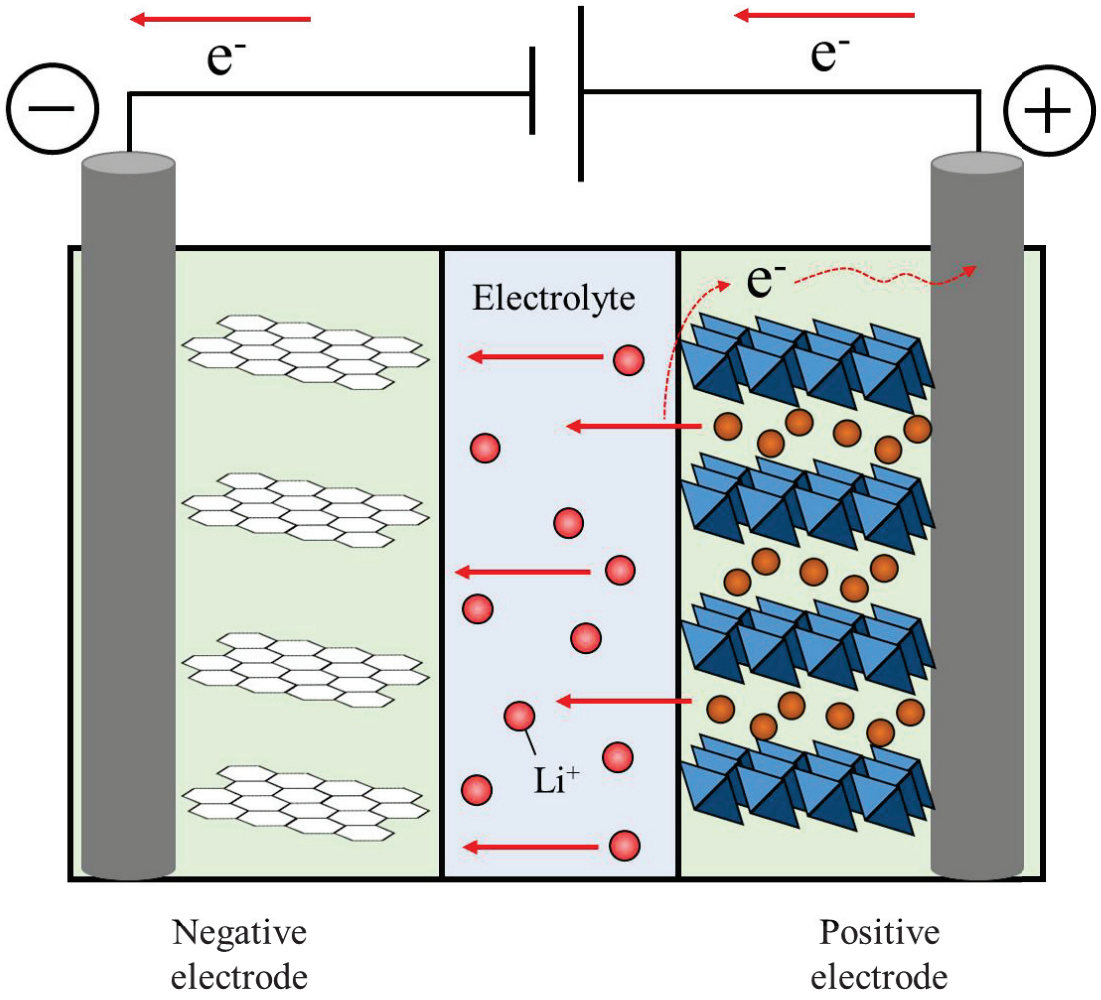

Figure 1-3 Schematic diagram of charging process for lithium-ion-batteries. The brown spheres indicate lithium atoms, and the red spheres indicate lithium ions. When current is transferred by an external charging power source, lithium ions escape from the crystal structure of the positive electrode to the electrolyte and are intercalated between the carbon crystal layers of the negative electrode.

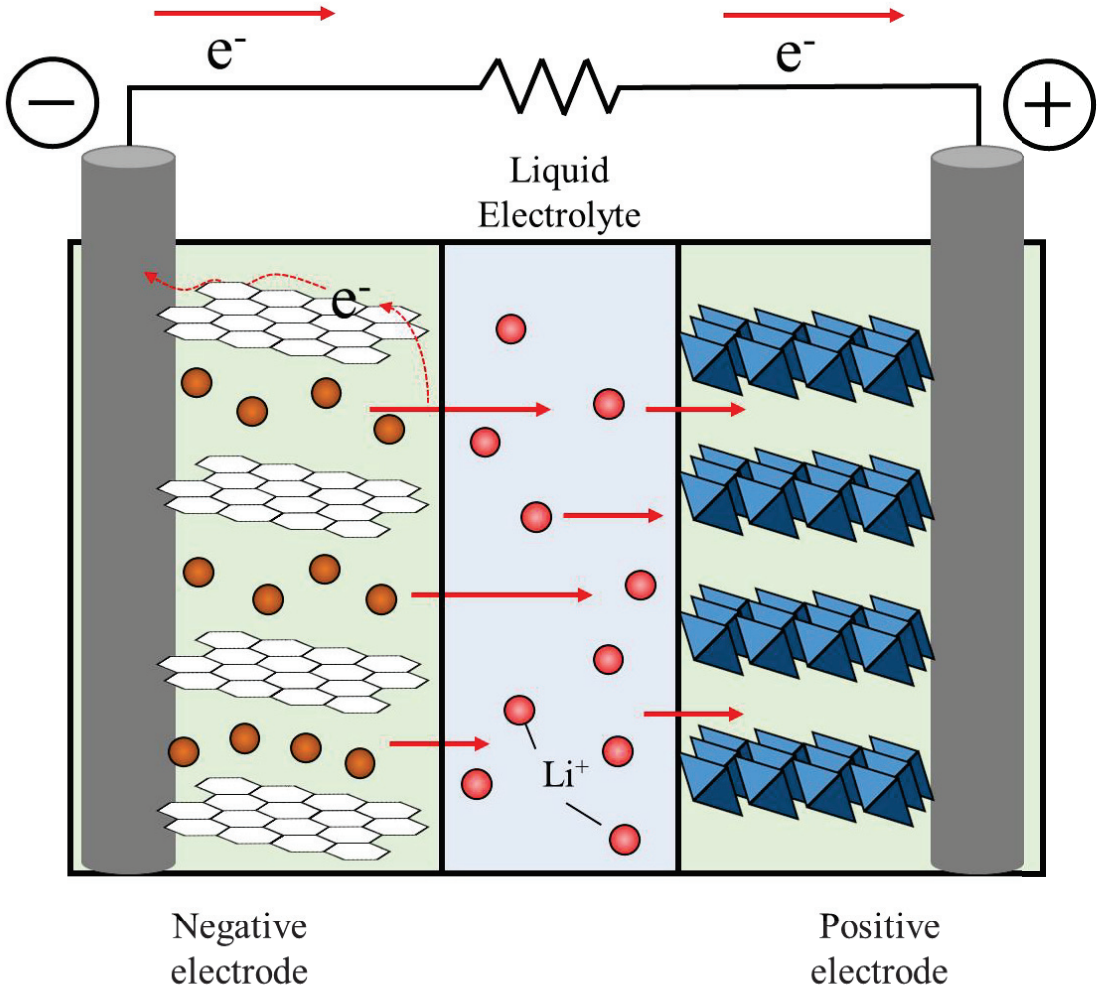

Figure 1-4 Schematic diagram of discharging process for lithium-ion-batteries. The brown spheres indicate lithium atoms, and the red spheres indicate lithium ions. When lithium ions escape from the carbon crystal layers of the negative electrode to the electrolyte and are inserted into the crystal structure of the positive electrode, current is extracted to an external circuit and the load functions.

1.4 Positive electrode materials

The voltage of the battery is determined by the difference between the reaction potentials of the positive and negative electrodes. Therefore, from the viewpoint of energy density, when the same negative electrode material is used, higher energy can be obtained as the reaction potential of the positive electrode is higher. The same can be said for the battery capacity. Physical properties of representative positive electrode materials are summarized in Table 1-1.

Lithium cobalt oxide is a positive electrode material that is widely used for batteries for mobile phones and conventional lithium-ion-batteries. The average operating voltage is about 3.7 **V**. Lithium manganesium oxide is a positive electrode material with improved capacity and safety of lithium cobalt oxide. It is mainly used as an electric vehicle battery. The average operating voltage is about 3.7 **V** similar to the cobalt system. Lithium iron phosphate has greatly improved safety and life characteristics compared with lithium cobalt oxide and lithium manganesium oxide. Since the lithium iron phosphate has an olivine crystal structure, it is also referred to as an olivine based positive electrode material. The average operating voltage is as low as 3.2 **V** compared to other lithium-ion-batteries.

Table 1-1 Material properties of typical positive materials [1-10].

Material composition	Average reaction potential [V vs Li^+/Li]	Theoretical Capacity [mAh/g]
$LiCoO_2$	3.8	274
$LiNiO_2$	3.8	275
$LiMn_2O_4$	4.1	148
$LiFePO_4$	3.4	170
$LiMnPO_4$	3.8	171
$LiNi_{0.8}Co_{0.15}Al_{0.05}O_2$	3.7	279

1.5 Negative electrode materials

The electrode material with the highest theoretical capacity is lithium metal. Its theoretical capacity is 3860 mAh/g. This is about 10 times the capacity of graphite described below. In addition, the standard electrode potential of lithium metal is –3.04 **V**, the operating voltage is high and the energy density can be increased. However, batteries using lithium metal as an electrode material have a safety problem. The reason is that dendritic lithium metal precipitates when charged, causing a short circuit with the positive electrode and there is a danger of ignition. For that reason, researches on electrode materials having safe and high capacity in place of lithium metal have been actively conducted in general.

From the previous studies, the negative electrode material of lithium-ion-batteries can be divided into three categories. An intercalation type such as graphite, an alloy type such as silicon, and finally a conversion type such as a metal hydride like MgH_2. A detailed explanation of each is given below.

1.5.1 Intercalation / de-intercalation type negative electrodes

A representative intercalation type material is graphite. The reaction mechanism between graphite and lithium ion has been extensively studied so far. The reaction mechanism is represented by the formula (1-11), Li ion is incorporated into the carbon by charging, and Li ions in carbon are released at the time of discharge. Figure 1-5 shows schematic diagram of Li insertion stages into graphite. Graphite electrodes charge and discharge according to the various insertion stages of Li ions. This representation is based on the Daumas-Hérold intercalated model [1-12, 1-13]. According to the previous studies, the insertion stages of Li into graphite are classified into four processes. They are classified into LiC_{72}, LiC_{36}, LiC_{12} and LiC_6. The insertion stage is defined according to the numbers of graphite layer which periodically separate the two Li atomic layers. For example, stage 4 corresponds to a crystalline phase in which there are four graphite layers between two Li layers. In the case of stage 1, the structure corresponds to the phase LiC_6 according to the stack A-α-A-α (A for the carbon layer, α for the Li layer). When LiC_6 is formed, the graphite electrode is fully charged. The theoretical capacity of LiC_6 is 372 mAh/g. Since the reaction potential is about 0.1 **V**, dendrites are not generated [1-11]. One Li ion will be inserted into the six carbons. On the other hand, in the case of a carbon

material having low crystallinity or orientation, an insertion reaction different from intercalation is observed, sometimes referred to as a dope reaction. In that case, LiC_2 and/or something like this are formed, and the result that the charge capacity exceeding 1000 mAh/g has been confirmed [1-14].

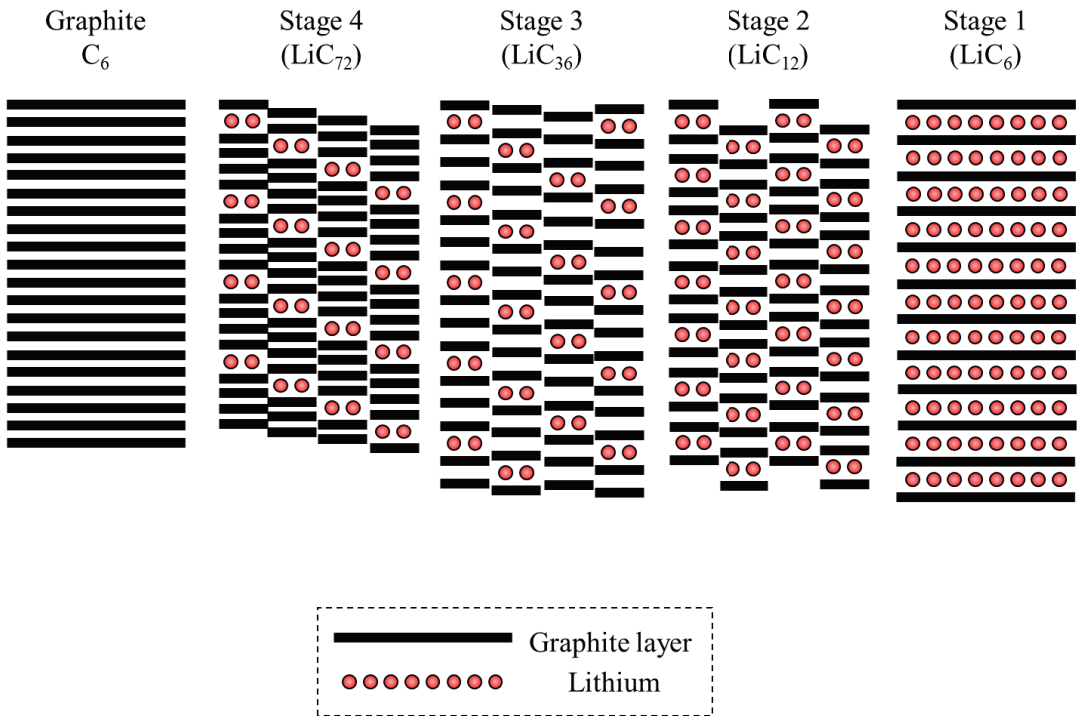

Figure 1-5 Schematic diagram of Li insertion stages into graphite and based on the Daumas-Hérold model [1-12, 1-13].

1.5.2 Alloying / de-alloying type negative electrodes

Over the past decade or more, researches on the study of negative electrode materials for a number of lithium-ion-batteries with high storage capacity and cycle characteristics exceeding the charge capacity of graphite of 372 mAh/g are proceeding. Among them, silicon (Si) has attracted much attention as an alternative material [1-15]. It has an excellent charge capacity of 4200 mAh/g and low operating potential of 0.5 **V**. Silicon reacts with Li ions and is known to form intermetallic states such as $Li_{12}Si_7$, $Li_{13}Si_4$, $Li_{22}Si_5$. However, when silicon is applied to a negative electrode material, Si particles proceeds due to a volume change（> 300%）accompanying reaction with Li ions. Cycle characteristics decrease and destruction and formation of the interface of the solid electrolyte are repeated as the nanostructure of the silicon shrinks during the charge and discharge cycles, the problem of thickening of the solid electrolyte interface (SEI) film remains [1-16].

Research resulting on silicon-based carbon composite materials has been reported to solve these volume change problems. Liu *et al.* have reported core/shell structure type, where the core is Silicon and shell is carbon, with excellent charge capacity and cycle characteristics [1-17].

1.5.3 Conversion type negative electrodes

Metal hydrides have been extensively studied in the field of hydrogen storage alloys for a long time. In recent years, studies have been reported on application to the negative electrode material of lithium-ion-batteries [1-18, 1-19, 1-20, 1-21, 1-22]. Metal hydrides are classified as conversion type negative electrode materials. The reaction shown in the following formula proceeds.

$$MH_x + xLi^+ + xe^- \rightarrow M + xLiH \qquad (1\text{-}13)$$

M = Metal (Mg, Ti, Na, Zr, etc.).

As shown in the above formula, the active material (MH_x) changes to a different material or disproportionates (LiH and M) with charge and discharge. When it charges and discharges again, the electrode reaction system returning to the state of the original active material is called a conversion reaction. The Gibbs free energy of this reaction is represented by the following formula.

$$\Delta_f G^\circ = [\Delta_f G^\circ(\mathrm{M}) + x\Delta_f G^\circ(\mathrm{LiH})] - [\Delta_f G^\circ(\mathrm{MH}_x) + x\Delta_f G^\circ(\mathrm{Li})] \quad (1\text{-}14)$$

$$= x\Delta_f G^\circ(\mathrm{LiH}) - \Delta_f G^\circ(\mathrm{MH}_x) \quad (1\text{-}15)$$

Since it is generally said that the formation energy of a metal, $\Delta_f G^\circ(M)$ and $\Delta_f G^\circ$(Li), defined to be 0, the equation (1-14) is converted to the equation (1-15). Conversion reaction between MH_x and Li proceeds as long as the condition that the result of the above equation is positive is satisfied. The theoretical reaction potential can be estimated from the Nernst equation.

Nernst equation is expressed as follows,

$$E = -\{\Delta_f G^\circ(2\mathrm{LiH}+\mathrm{M}) - \Delta_f G^\circ(\mathrm{MH}_x+2\mathrm{Li})\}/2F, \quad (1\text{-}16)$$

where F is Faraday constant. For example, when $E < 0$, Li will precipitate on the electrode before proceeding of the target reaction, so the reaction does not proceed. As described above, if the standard generated Gibbs energy of the metal hydride is determined, the

reaction potential derived from the Nernst equation can be derived as shown in Figure 1-5.

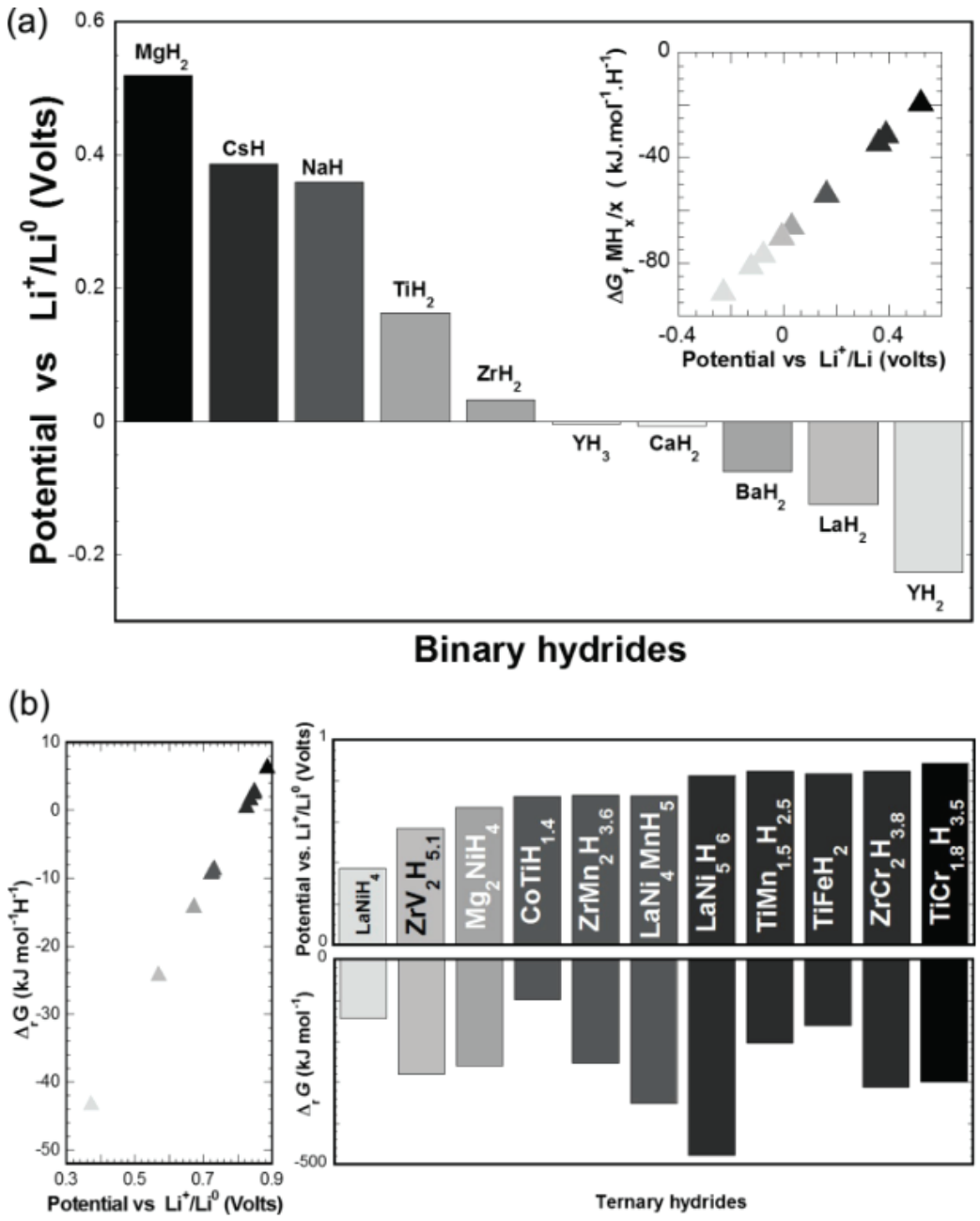

Figure 1-6 Theoretical equilibrium potential for the MH_x/Li cell vs Li^+/Li. [1-23]

Figure (a) shows the relationship between the standard Gibbs energy of binary hydride and the reaction potential derived from the Nernst equation, and figure (b) shows the case of ternary hydride.

1.6 Liquid electrolyte

The electrolyte plays an important role in the ion movement between the positive electrode and the negative electrode. Electrochemical properties such as high ionic conductivity, high lithium ion ration, oxidation resistance, reduction resistance, and a small emissive mobility resistance at the electrode interface are required. An electrolytic solution prepared by dissolving $LiPF_6$ in a solvent mixed with an ethylene carbonate (EC) and a dialkyl carbonate (DAC) ester is used as a current lithium-ion-battery. Development of polymer electrolytes and inorganic solid electrolytes with no concern of leakage is underway other than liquid electrolytes.

An electrolyte composed of an electrolyte salt and an organic solvent is used in the most commercially available lithium-ion-batteries. Generally, a supporting electrolyte such as $LiPF_6$ or $LiBF_4$ is used. Dimethyl carbonate（DMC）, propylene carbonate（PC）, or something like these are used as the electrolyte solvent. The liquid electrolyte is characterized by excellent ion conductivity. On the other hand, problems such as ignition due to leakage and other safety issues remain.

Recently studies using substances consisting of ionic bond materials in a liquid state so called ionic liquids are in progress gradually. The ionic liquid has an advantage with

respect to the electric conductivity, possessing higher as compared with the ordinary electrolytic solution. An imidazolium salt, which is famous as a cation constituting an ionic liquid, shows the highest electrical conductivity at room temperature. Furthermore, since the general electrolytic solution is a flammable liquid and the ionic liquid is composed only of ions, it has almost no vapor pressure and is a flame retardant / incombustible liquid. However, problems to be solved such as lifetime as a battery material remain [1-24].

1.7 All-solid-state lithium-ion-batteries

An all-solid-state lithium-ion-battery using an incombustible inorganic solid electrolyte has attracted attention as a next generation electric storage device, in place of a conventional lithium-ion-battery using a flammable organic electrolytic solution. By using a nonflammable solid electrolyte, ignition due to liquid leakage is suppressed, which is a highly safe battery.

Furthermore, in the case of a liquid electrolyte, pyrolysis readily occurs when it works at high temperatures, so the operating temperature was limited. On the other hand, in the case of an all solid state battery, since the thermal stability of the solid electrolyte is high, there is a merit that the operating temperature range is wide. However, in the all-solid-state batteries, the migration resistance of the Li ions of the electrolyte is higher than that of the conventional lithium-ion-battery. And, the contact resistance between electrode and the electrolyte is also high, so that the increase in internal resistance is one of the problems. Figure 1-7 shows schematic diagram of operating principle for all solid state lithium-ion-batteries.

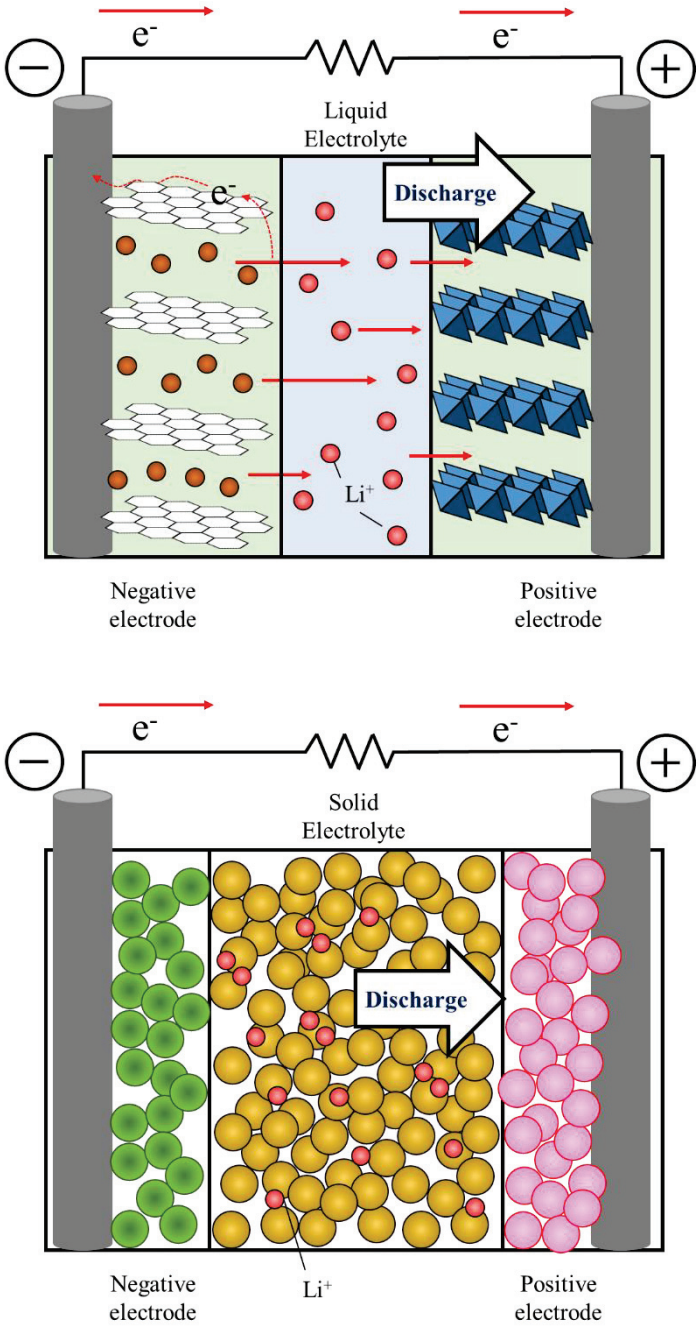

Figure1-7 Schematic diagram of lithium ion batteries using liquid electrolyte and solid electrolyte (Top: liquid type lithium-ion-battery, Bottom: all-solid-state lithium-ion-battery).

1.8 Solid electrolytes

A lithium-ion-battery using a solid material instead of a conventional liquid is called an all-solid-state batteries. Technical advantages of all-solid-state batteries are: (1) high safety, (2) no leakage, (3) difficult to ignite, (4) low possibility of short-circuiting the positive and negative electrodes, and the like. Furthermore, it is also a great advantage that ion conductivity at high temperature around 150 °C is high. In recent years, various materials have been studied as candidate materials for lithium ion conductors. For example, oxides [1-25, 1-26], sulfide based crystals and glasses [1-27, 1-28], multi-metal halides and composite type electrolytes are expected for the solid state electrolytes [1-29]. The lithium ion conductors are briefly summarized as follows.

1.8.1 Lithium iodide (LiI)

The search for lithium conductors began around the 1970's, and lithium halides of LiX (X = F, Cl, Br, I) were the first. The crystal structure of LiI is a NaCl type structure similar to the other lithium halides, but since the polarization of I^- ions is large, its ionic conductivity of 10^{-7} S/cm is developed. This was a very low ionic conductivity compared to liquid, but in 1972 it was put to practical use as an electrolyte for pacemaker batteries.

1.8.2 Lithium nitride (Li_3N)

Lithium nitride, Li_3N, attracted interest because of its high Li content and its open structure buildup of sequential Li and Li_2N layers [1-30]. Despite these efforts, Li_3N which was discovered in the 1970s still has the highest ionic conductivity (6×10^{-3} S/cm at room temperature) of potential solid electrolytes. The crystal structure of Li_3N was initially proposed by Zintl and Brauer [1-31] and reevaluated by Rabenau and Schuh [1-32, 1-33].

Li_3N (space group P6/mmm) can be considered as a layered structure with Li_2N layers perpendicular to the hexagonal c axis. From this structural arrangement of Li_3N it can be deduced that the thermal motion of the Li atoms should take place preferentially in the Li layers perpendicular to the Li-N bonds. However, the low decomposition potential of 0.445 **V** restricts its application as a lithium solid electrolyte [1-34, 1-35].

1.8.3 Lithium super ionic conductor (LISICON)

In the lithium ion conductors, there is an oxide substance group called LISICON (Lithium super ionic conductor) [1-36]. It is a generic term attached to an ionic conductor represented by $x\mathrm{Li_4Ge_{4-(1-x)}Zn_2Ge_4}$ in which Zn is solid-solution in a material having $\mathrm{Li_4Ge_4O_4}$ as a mother structure. By substituting ions of different valences, it is easy to introduce Li defects and excess Li and is characterized by various structures and composition changes. A representative material is $\mathrm{Li_{(3+x)}P_{(1-x)}Ge_xO_4}$ in which interstitial Li is introduced by partial substitution of P^{5+} with Ge^{4+}.

LISICON is a kind of oxide-based materials. In order to further improve ionic conductivity, it was next considered to use sulfur with a high polarizability instead of oxygen. Kanno and Irie *et al.* have searched for a group of substances based on germanium sulfide such as $\mathrm{Li_2S\text{-}GeS_2}$, $\mathrm{Li_2S\text{-}GeS_2\text{-}ZnS}$, $\mathrm{Li_2S\text{-}GeS_2\text{-}Ga_2S_3}$, etc. Kanno and colleagues named this material system as Thio-LISICON by adding "Thio" indicating sulfide to oxide LISICON. Moreover, Murayama *et al.* discovered a material of $\mathrm{Li_{(2-x)}Ge_{(1-x)}P_xS_4}$ solid solution of 2.2×10^{-3} S/cm [1-37, 1-38]. As a summary, Figure 1-8 shows temperature dependence of ionic conductivity of representative lithium ion conductors.

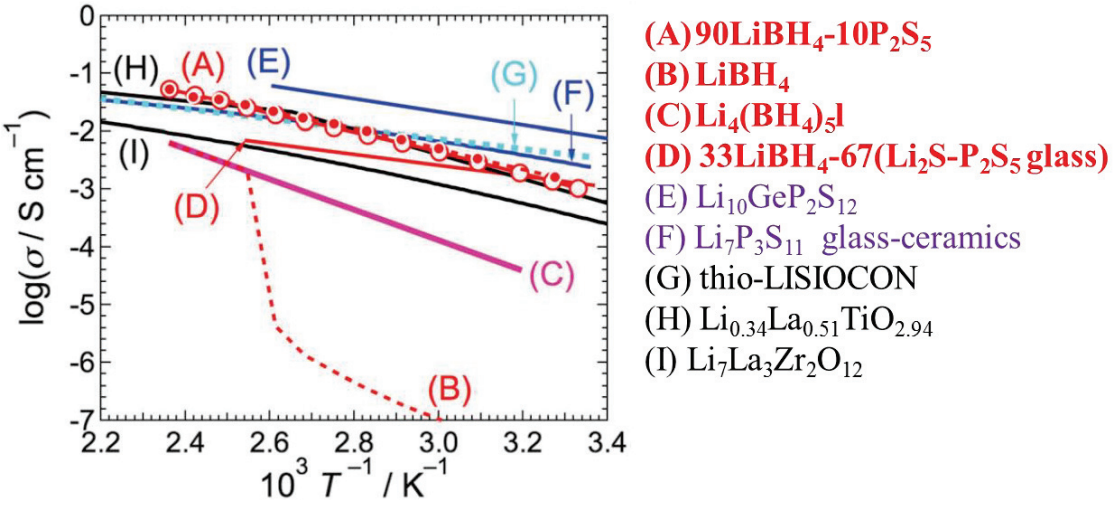

Figure 1-8 Temperature dependence of ionic conductivity of representative lithium ion conductor [1-39, 1-40].

1.8.4 Lithium borohydride ($LiBH_4$)

$LiBH_4$ has been extensively studied as a candidate for hydrogen storage materials. In 2007, Matsuo *et al.* reported $LiBH_4$ shows excellent lithium ion conductivity [1-41]. As the temperature rises, $LiBH_4$ undergoes a structural phase transition from a tetragonal phase which is a low temperature phase to a hexagonal phase which is a high temperature phase in the vicinity of 390 K [1-42] as shown in Figure 1-9. This high temperature phase shows excellent lithium ion conductivity. However, batteries using $LiBH_4$ as a solid electrolyte are limited to operating temperatures of 390 K or more, which is the phase transition temperature. In order to solve this problem, in 2009, Maekawa and colleagues examined a method of stabilizing the high temperature phase to the low temperature region by dissolving lithium halide such as lithium iodide in $LiBH_4$. As a result, it was reported that $Li_4(BH_4)_3I$ exhibits excellent ion conductivity even in a low temperature region of 300 K [1-43]. In fact, there is a lithium-ion-battery in which a metal hydride MgH_2 is applied as an electrode material assuming that an all-solid-state battery is manufactured using $LiBH_4$ as a solid electrolyte and electrochemical characteristics are reported. It has been clarified that application of $LiBH_4$ and MgH_2 to solid electrolytes and electrode materials improves the conductivity of hydrogen ions in MgH_2 [1-44].

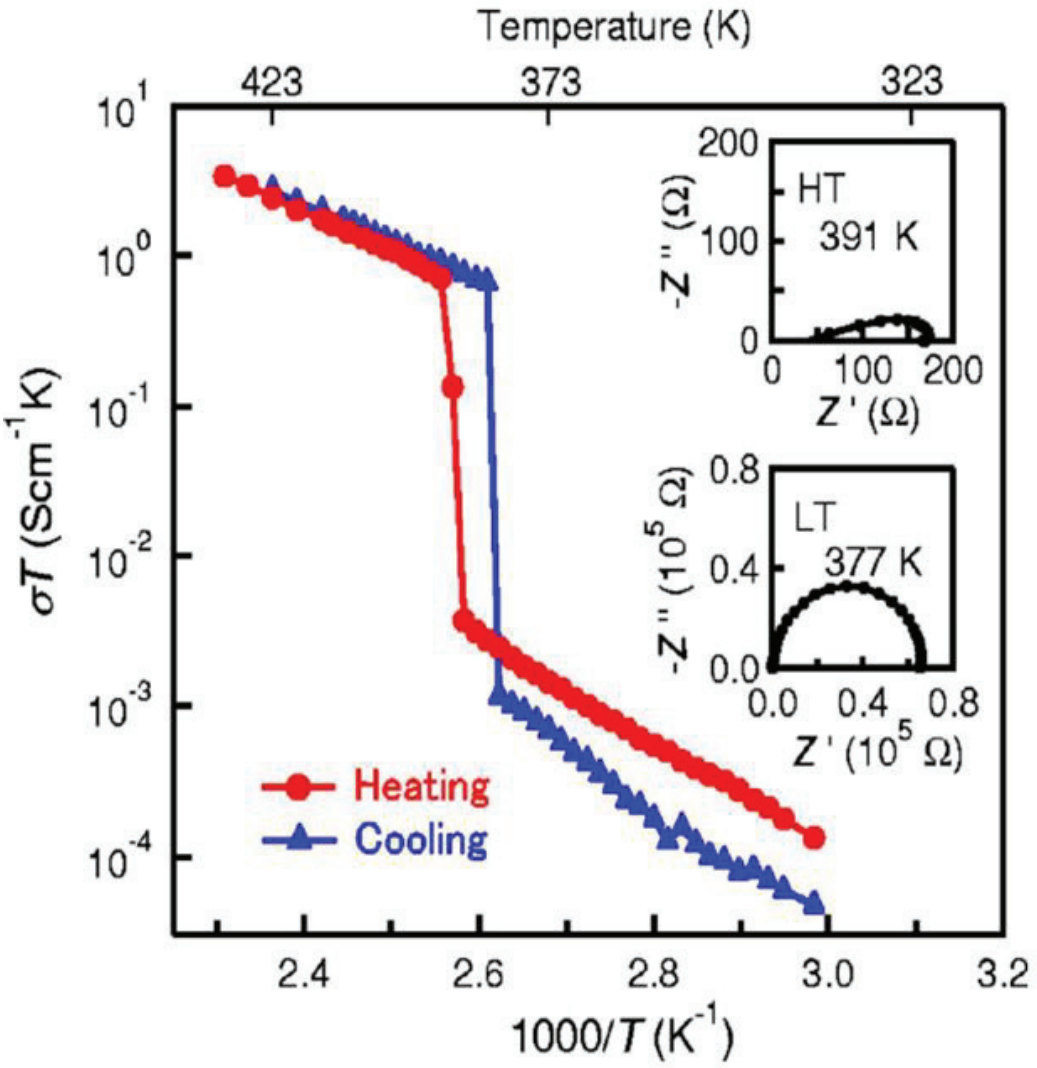

Figure 1-9 Ionic conductivity of $LiBH_4$ [1-41]. The horizontal axis indicates temperature, and the vertical axis indicates ionic conductivity. The red line shows the result of measuring the ionic conductivity with increasing temperature. The blue line shows the result of cooling and measuring. The insets show plots of complex impedance measured at 377 K (LT) and 391 K (HT).

1.9 Hydrogen storage properties for vanadium hydride

1.9.1 Vanadium-hydrogen system

Vanadium metal with a bcc structure has attracted attention as a candidate for hydrogen storage material from its high hydrogen storage capacity (3.8 weight%) [1-45]. Vanadium metal is usually called α phase. And Vanadium metal forms β phase (V_2H) at the beginning when hydrogen is adsorbed. Thereafter, when hydrogen is adsorbed further, a γ phase (VH_2) is formed. That is, in the VH system, two plateaus appear in the PC (pressure-composition) isothermal curve. First of all, a reaction that can make a β phase as shown by the following equation occurs.

$$2V\ (\alpha) + 1/2\ H_2 \Leftrightarrow V_2H\ (\beta) \qquad (1\text{-}17)$$

After that, when the reaction further proceeds, the reaction of the following formula occurs, and a γ phase is formed.

$$V_2H\ (\beta) + 1/2\ H_2 \Leftrightarrow VH_2\ (\gamma) \qquad (1\text{-}18)$$

The β phase is very stable and no release reaction of hydrogen takes place under normal circumstances [1-46]. On the other hand, the γ phase is very unstable, and the hydrogen adsorption and release reaction are occurred under hydrogen atmosphere. Hydrogenation of V proceeds easily with moderate temperature after an appropriate activation. In order to improve the stability of the γ phase, alloying by elements has been extensively studied [1-47, 1-48, 1-49, 1-50]. The total reaction of hydrogenation for V is shown as PC isothermal properties in Figure 1-10. Figure 1-11 shows PC isothermal curves for V at high hydrogen pressures measured in the course of hydrogenation at 313 K.

As mentioned above, the V-H system exists in various hydride states depending on the conditions. The reason why the crystal structure of vanadium hydride has not been determined is the difficulty of analysis. For example, it is difficult to detect hydrogen when using X-ray diffraction method. Vanadium is difficult to be detected when neutron diffraction method is used. Therefore, the crystal structure of vanadium hydride has not been determined exactly.

1.9.2 Body-centered-cubic metal solid solutions

In general, hydrogen reacts with all elements except rare gases. As a result, it can be roughly classified into three types of hydrides. There are three types: ion-bonded hydrides, metal-bonded hydrides, and covalent-bonded hydrides. When hydrogen reacts with alkali metals and alkaline earth elements, the ion-bonded hydrides are formed. When hydrogen reacts with the 3B-7B group element, the covalent-bonded hydrides are formed. Group 3A-8 transition element hydrides containing the vanadium, lanthanoid, and actinoid elements listed above are classified as metal-bonded hydrides.

These metal-bonded hydrides are usually black powders that do not lose their metal properties. The bonding state of hydrogen ranges from ionic bonds to metal bonds. The stronger the ionic bond, the more stable the hydride. It is possible to keep hydrogen up to the high temperature range. In hydrides with strong metal bonds, hydrogen dissolves in the form of H^+. Then, hydrogen is easily released in a low temperature region where the bonding property with the metal element is weak and becomes a metal. Since hydrogen atoms have a small atomic radius, they enter the gap of the metal lattice. Therefore, the oxidation number of hydrogen is zero. The 5A group elements, such as vanadium (V), niobium (Nb), and tantalum (Ta), dissolve hydrogen in the interstitial position of the

Body-centered-cubic (BCC) structure of the metal element [1-51]. And hydrides are formed over a wide composition range. The continuous transition from the metal phase to the hydride phase occurs with a relatively slight increase in temperature. Iba *et al.* has revealed that among the alloys based on titanium (Ti) and V, the solid solution phase with BCC structure has a much higher hydrogen storage capacity than conventional alloys. For example, the Ti-V-Mn alloy showed an excellent hydrogen release of 2.1 weight% at 1000 °C. Ti-V-Cr and Ti-V-Cr-Mn alloys have also been developed and these alloys are called "Laves phase related BCC solid solution".

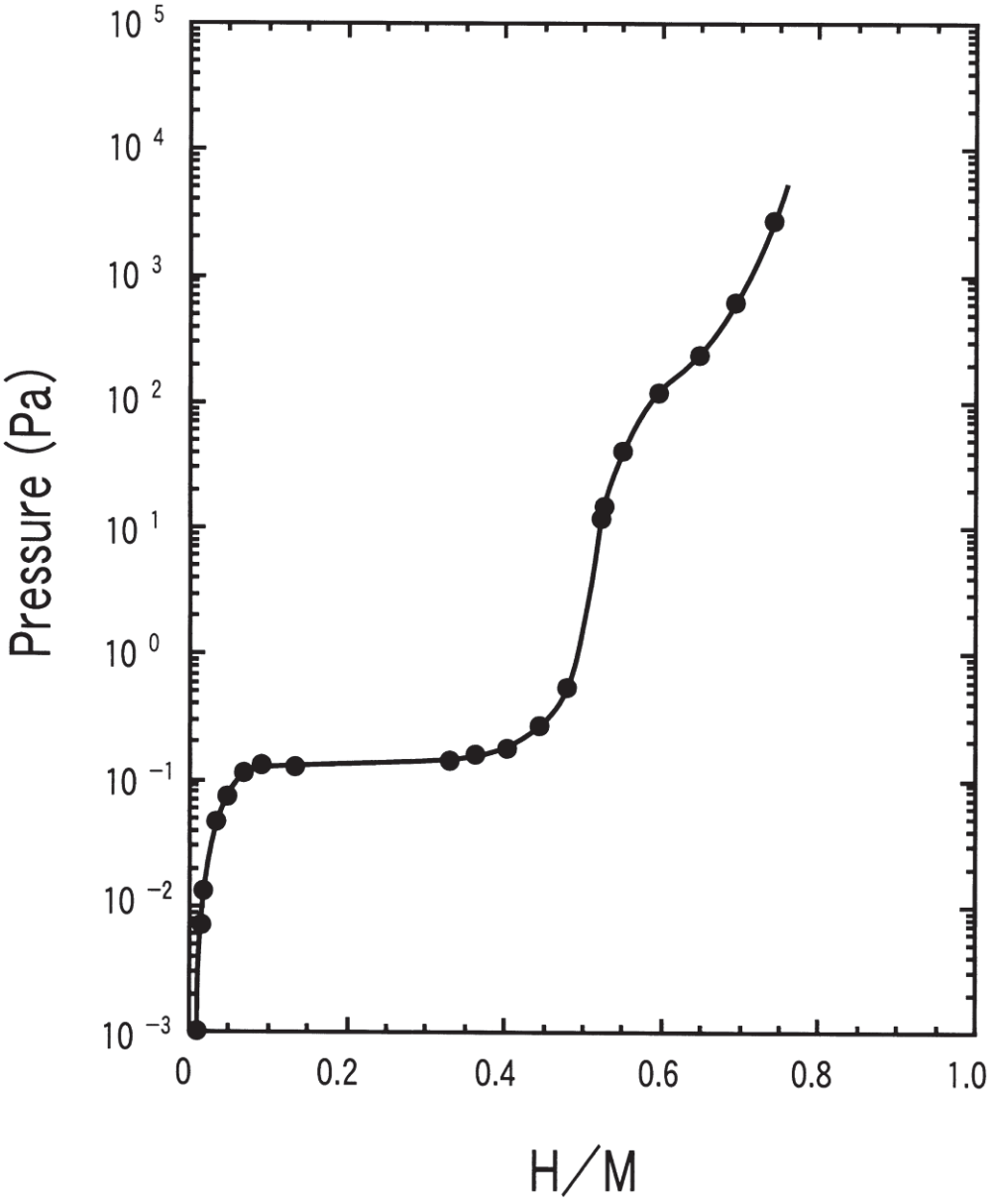

Figure 1-10 PCT curve for pure vanadium measured at low hydrogen pressures in the course of hydrogenation at 343 K [1-52]. The horizontal axis is the atomic ratio of the absorbed hydrogen and the metal constituting the alloy. The vertical axis indicates the pressure of hydrogen.

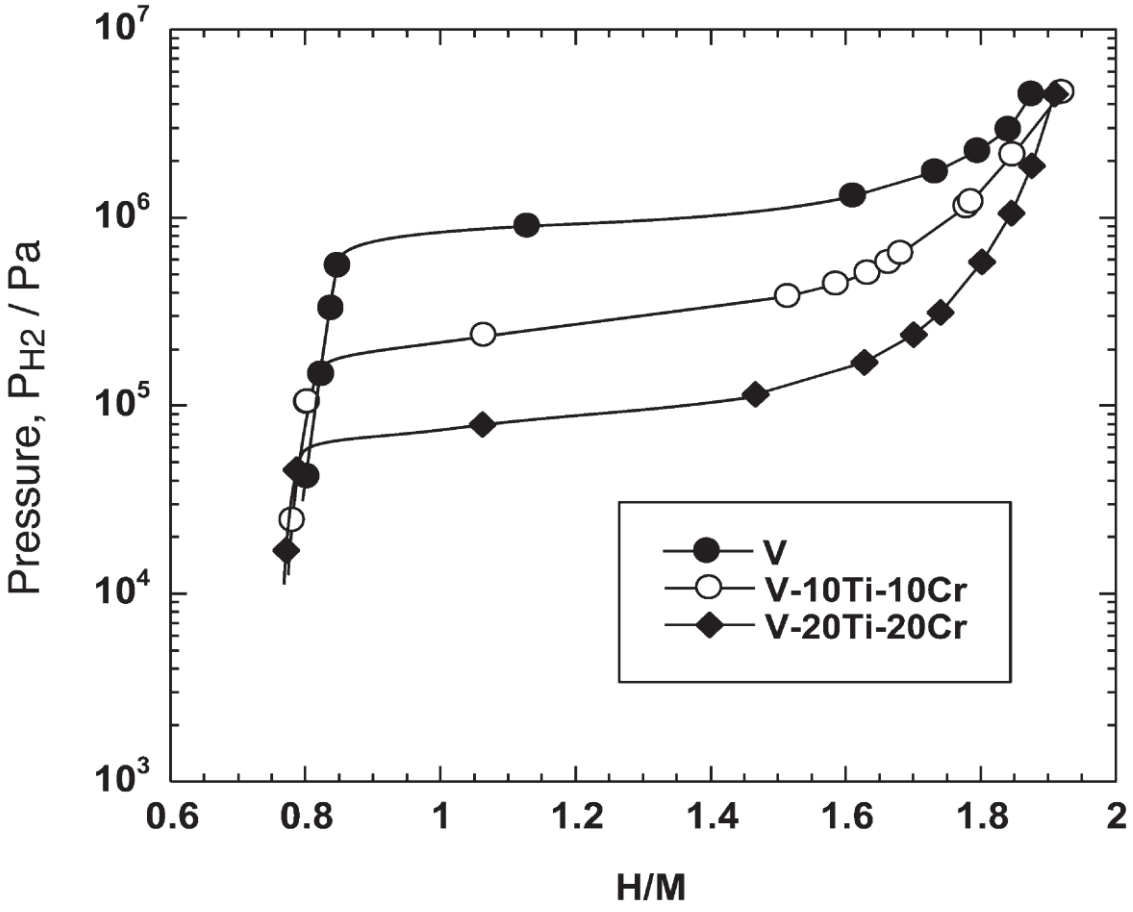

Figure 1-11 PCT curves for vanadium at high hydrogen pressures measured in the course of hydrogenation at 313 K [1-53]. The horizontal axis is the atomic ratio of the absorbed hydrogen and the metal constituting the alloy. The vertical axis indicates the pressure of hydrogen.

References

[1-1]

http://www.meti.go.jp/committee/sankoushin/sangyougijutsu/chikyu_kankyo/yakusoku_souan_wg/pdf/007_s01_00.pdf

[1-2]

http://www.enecho.meti.go.jp/about/special/tokushu/ondankashoene/pariskyotei.html

[1-3]

http://www.enecho.meti.go.jp/committee/council/basic_policy_subcommittee/mitoshi/pdf/report_01.pdf

[1-4] N. Achaibou, M. Haddabi and A. Malek: *Journal of Power Sources* 185 (2008) 1484-1491.

[1-5] T. Oshima, M. Kajita and A. Okuno: *International Journal of Applied Ceramic Technology* 1 (2004) 269-276.

[1-6] Z. Wen, Y. Hu, X. Wu, J. Han and Z. Gu: *Advanced Functional Materials* 23 (2013) 1005-1018.

[1-7] https://eco-word.jp/html/04_energy/en-17.html

[1-8] T. Sakai, H. Ishikawa, K. Oguro, C. Iwakura and H. Yoneyama: *Journal of The*

Electrochemical Society 134 (1987) 558-562.

[1-9] J.M. Tarascon and M. Armand: *Nature* 414 (2001) 359-367.

[1-10] H. Saruwatari: *Journal of the Japan Society of Applied Electromagnetics and Mechanics* 24 (2016) 287-292.

[1-11] M. Endo, J. Nakamura, Y. Sasabe, T. Takahashi and M. Inagaki: *Tanso*, 165 (1994) 282-287.

[1-12] D. Allart, M. Montaru and H. Gualous: *Journal of The Electrochemical Society* 165 (2018) A380-A387.

[1-13] V. A. Sethuraman, L. J. Hardwick, V. Srinivasan and R. Kostecki: *Journal of Power Sources* 195 (2010) 3655–3660.

[1-14] K. Sato, M. Noguchi, A. Demachi, N. Oki and M. Endo: *Science* 264 (1994) 556-558.

[1-15] X. Zuo, J. Zhu, P. Müller-Buschbaum and Y.-J. Cheng: *Nano Energy* 31 (2017) 113-143.

[1-16] H. Wu and Y. Cui: *Nano Today* 7 (2012) 414-429.

[1-17] N. Liu, H. Wu, M. T. McDowell, Y. Yao, C. Wang and Y. Cui: *Nano Letters* 12 (2012) 3315-3321.

[1-18] Y. Oumellal, A. Rougier, J.-M. Tarascon and L. Aymard: *Journal of Power Sources*

192 (2009) 608-702.

[1-19] L. Huang, L. Aymard and J.P. Bonent: *Journal of Materials Chemistry A* 3 (2015) 15091-15096.

[1-20] S. Brutti, G. Mulas, E. Picillo, S. Panero and P. Reale: *Journal of Materials Chemistry* 22 (2012) 14531–14537.

[1-21] S. Ikeda, T. Ichikawa, K. Kawahito, K. Hirabayashi, H. Miyaoka and Y. Kojima: *Chemical Communications* 49 (2013) 7174-7176.

[1-22] P. Lopez-Aranguren, N. Berti, A. Ha Dao, J. Zhang, F. Cuevas, M. Latroche and C Jordy: *Journal of Power Sources* 357 (2017) 56-60.

[1-23] L. Aymard, Y. Oumellal and J.P. Bonnet: *Beilstein Journal of Nanotechnology* 6 (2015) 1821-1839.

[1-24] H. Tokuda, S. Kinoshita and M. Ue: *Journal of the Surface Science Society of Japan* 28 (2007) 327-332.

[1-25] H. Aono, N. Imanaka and G. Adachi: *Accounts of Chemical Research* 27 (1994) 265–270.

[1-26] Y. Inaguma, C. Liquan, M. Itoh, T. Nakamura, T. Uchida, H. Ikuta and M. Wakihara: *Solid State Communications* 86 (1993) 689-693.

[1-27] M. Tachez, J.P. Malugani, R. Mercier and G. Robert: *Solid State Ionics* 14 (1984)

181-185.

[1-28] M. Tatsumisago, H. Yamashita, A. Hayashi, H. Morimoto and T. Minami: *Journal of Non-Crystalline Solids* 274 (2000) 30-38.

[1-29] H. Maekawa, R. Tanaka, T. Sato, Y. Fujimaki and T. Yamamura: *Solid State Ionics* 175 (2004) 281–285.

[1-30] F. W. Poulsen, N. H. Andersen, B. Kindl and J. Schoonman: *Solid State Ionics* 119 (1983) 9-10.

[1-31] E. Zintl and G. Brauer: *Zeitschrift für Elketrochemie* 41 (1935) 102.

[1-32] U. V. Alpen, A. Rabenau and G.H. Talat: *Applied Physics Letters* 30 (1977) 621-623.

[1-33] A. Rabenau and H. Schulz: *Journal of the Less Common Metals* 50 (1976) 155.

[1-34] R. A. Huggins: *Electrochem Acta*, 22 (1977) 773.

[1-35] M. Yonemura: *Journal of the Crystallographic Society of Japan* 57 (2015) 79-86.

[1-36] H. Y-P. Hong: *Materials Research Bulletin* 13 (1978) 117.

[1-37] M. Murayama, R. Kanno, Y. Kawamuto and T. Kamiyama: *Solid State Ionics* 789 (2002) 154-155.

[1-38] R. Kanno and M. Murayama: *Journal of The Electrochemical Society* 148 (2001) A742-A746.

[1-39] http://www.spring8.or.jp/ja/news_publications/research_highlights/no_49/

[1-40] A. Unemoto, H. Wui, T. J. Udovic, M. Matsuo, T. Ikeshoji and S. Orimo: *Chemical Communications* 52 (2016) 564-566.

[1-41] M. Matsuo, Y. Nakamori, S. Orimo, H. Maekawa and H.Takamura: *Applied Physics Letters* 91 (2007) 224103.

[1-42] J-Ph. Soulie, G. Renaudin, R. Cerny and K. Yvon: *Journal of Alloys and Compounds* 346 (2002) 200-205.

[1-43] H. Makekawa, M. Matsuo, H. Takamura, M. Ando, Y. Noda, T.Karahashi and S. Orimo: *Journal of the American Chemical Society* 131 (2009) 894-895.

[1-44] L. Zeng, K. Kawahito, S. Ikeda, T. Ichikawa, H. Miyaoka and Y. Kojima: *Chemical Communications* 51 (2015) 9773.

[1-45] J.J. Reilly and R.H. Wiswall: *Inorganic Chemistry* 9 (1970) 1678.

[1-46] K. Fujita, Y.C. Huang and M. Tada: *Journal of Japan. Institute of Metals and Materials* 43 (1979) 601.

[1-47] A.J. Mealand, G.G. Libowitz, J.F. Lynch and G. Rak: *Journal of the Less Common Metals* 104 (1984) 133.

[1-48] G.G. Libowitz and A.J. Mealand: *Materials Science Forum* 31 (1988) 177.

[1-49] A. Kagawa, E. Ono, T. Kusakabe and Y. Sakamoto: *Journal of the Less Common*

Metals 172-174 (1991) 64-70.

[1-50] H. Yukawa, M. Takagi, A. Teshima and M. Morinaga: *Journal of Alloys and Compounds* 330-332 (2002) 105 –109.

[1-51] C. Wainwright, A.J. Cook and B.E. Hopkins: *Journal of the Less Common Metals* 6 (1964) 362-374.

[1-52] H. Yukawa, A. Teshima, D. Yamashita, S. Ito, S. Yamaguchi and M. Morinaga: *Journal of Alloys and Compounds* 337 (2002) 264–268.

[1-53] H. Yukawa, D. Yamashita, S. Ito, M. Morinaga and S. Yamaguchi: *Journal of Alloys and Compounds* 356-357 (2003) 45–49.

2. Purpose

Metal hydrides have been studied as an electrode material for lithium ion batteries. In particular, metal hydrides such as MgH_2 are expected as negative electrode materials for lithium-ion-batteries. Therefore, numerous research results have been reported so far. Most of the research results using metal hydrides like MgH_2 and so on, as electrode materials reported have been investigated remarkably in organic electrolytic solution systems. In our group, we have focused on all-solid-state lithium-ion-batteries and have been conducting research. In particular, as a hydride, much research has been done since MgH_2 and VH_2 can control the hydrogen absorption / desorption reaction under comparatively mild conditions. From the past literature, in the case of MgH_2 and TiH_2, the correlation between the performance as a hydride and the battery characteristics has been well investigated. On the other hand, in the case of the VH_2 system, the thermodynamic performance as its hydrogen storage alloy has been well investigated, but the electrochemical performance is not well understood.

Therefore, in this study, we focus on vanadium as a hydride and clarify electrochemical characteristics of vanadium as a conversion type negative electrode. As a result, we aim to elucidate the correlation between the hydrogen storage / release

characteristics and the electrochemical characteristics which have been reported so far by characterizing the reaction. I want to approach the detailed reaction mechanisms about this.

3. Experiments

3.1 Materials

Starting materials used in this study are shown in Table 3-1. All the samples were handled in an Ar filled glove box (0.1 MPa, water and oxygen were less than 1ppm.) to avoid oxidation and water adsorption. $LiBH_4$ was used as a solid electrolyte, and acetylene black, a type of carbon fine particles, was used to improve electron conductivity.

Table 3-1 General information of materials.

Materials	Purity, State	Company
Vanadium (V)	99.9%, powder	Rare metallic
Lithium hydride (LiH)	99.4%, powder	Alfa Aesar
Lithium borohydride ($LiBH_4$)	95%, powder	Sigma Aldrich
Acethylene black	Powder	Hohsen Corp.
Lithium (Li)	99.8%, disc (φ:15 mm)	Honjo Metal

3.2 Synthesis of mixture electrode

Since VH_2 is an unstable material without proper pressure [3-1] as shown in Figure 3-1, a mixture of V and LiH was prepared as starting materials. V and LiH powders were mixed by mechanical ball-milling method with following procedure. V and LiH weighed in a molar ratio of 1: 3 (total 300 mg), and 20 pieces of zirconia balls (diameter: 8 mm) were put into a milling vessel (SKD-11, Cr steel). Milling treatment was performed for 2 h with 370 rpm under Ar gas pressure of 0.1 MPa by a planetary ball-milling apparatus (Fritsch, P7). Figure 3-2 shows schematic image of the planetary ball-milling apparatus.

The purchased $LiBH_4$ as a Li-ion conducting material was hand-milled in a mortar for 15 min. in order to increase the interface with the electrode materials. Then, the $LiBH_4$ powder and acetylene black were heated up to 200 °C and kept for 12 h under dynamic vacuum to remove adsorbed gases on the surface such as moisture before samples mixing. The V-LiH mixture was mixed with $LiBH_4$ and acetylene black as an electron conducting material in a weight ratio of 40: 30: 30 (total 200 mg) by the ball-milling for 2 h with 370 rpm under 0.1 MPa of Ar. Finally, an electrode active material that is a mixture of the V-LiH mixture, $LiBH_4$, and acetylene black was obtained. The crystal structure changes of the V-LiH mixture and the electrode material after each ball mill treatment were analyzed

using powder X-ray diffraction.

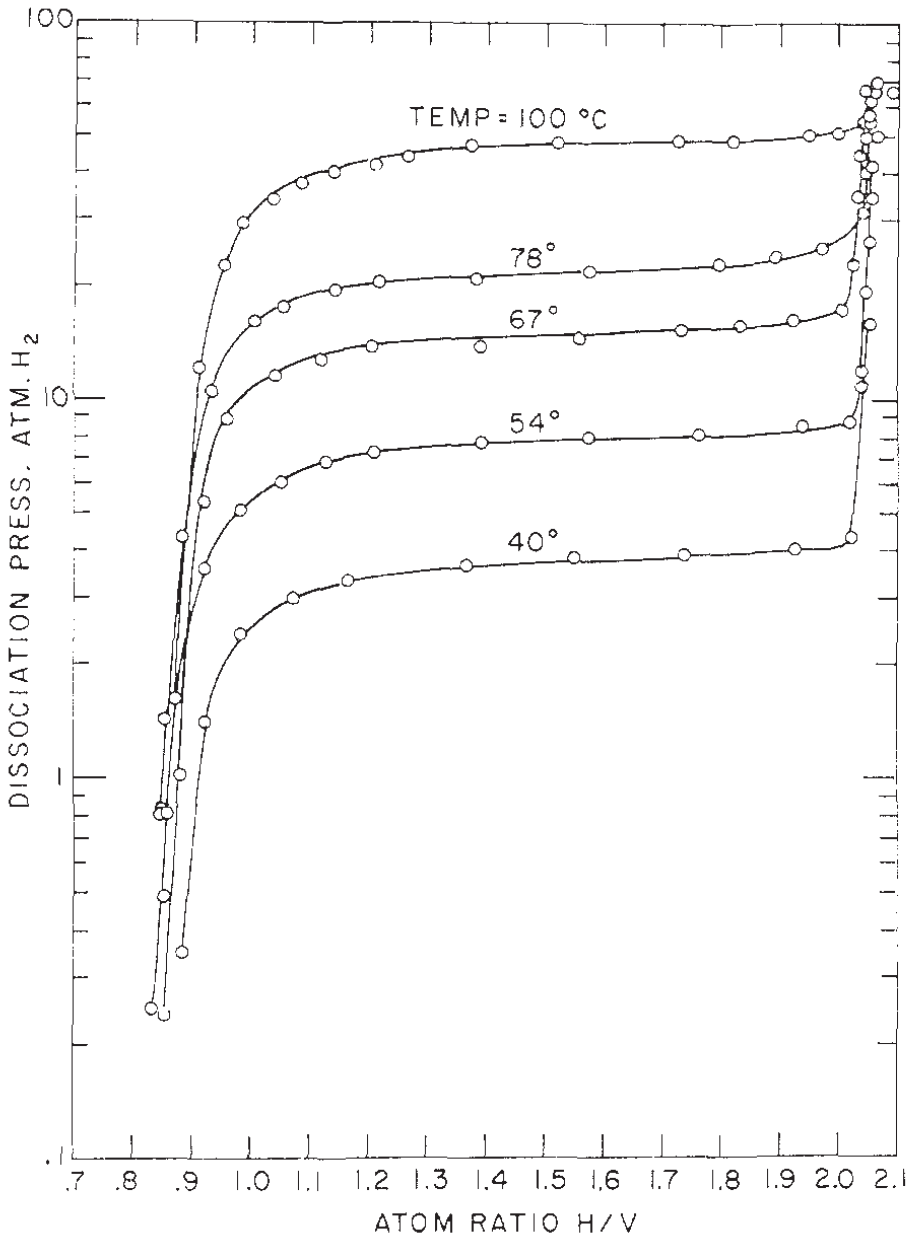

Figure 3-1 pressure-composition isotherms for the V_2H – VH_2 transformation [3-1].

"Reprinted (adapted) with permission from (COMPLETE REFERENCE CITATION). Copyright (2019) American Chemical Society."

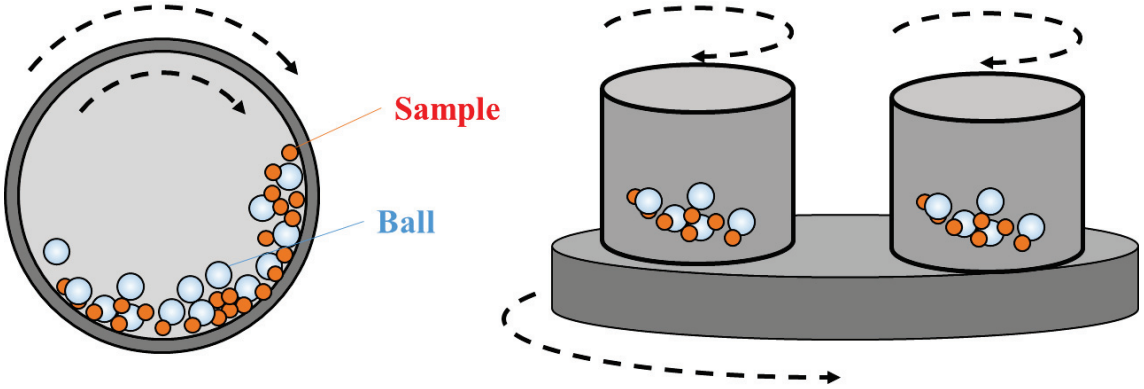

Figure 3-2 Schematic image of the planetary ball-milling apparatus.

3.3 Battery cell assembly

When evaluating the electrode characteristics of an all-solid-state lithium-ion-battery, the electrode characteristics strongly depend on the state of the electrode material, so it is necessary to create the electrode accurately. In particular, in the case of an all-solid-state lithium-ion-battery, the interface between the electrode material and the solid electrolyte is very important. If the interface between the electrode material and the solid electrolyte is not sufficiently contacted, the electron conductivity will decrease. As a result, the charge / discharge characteristics will not be obtained correctly. In general, a pellet maker is used to assemble an all-solid-state lithium-ion-battery test cells (Figure 3-3). By applying a high pressure, the contact within the electrode material and at the interface between the electrode material and solid electrolysis is tight.

Also, in the case of a lithium-ion-battery, to examine the material properties for each of the positive and the negative electrodes, a half-cell is widely used in the evaluation of electrode properties. In this cell, the material is evaluated on the positive electrode side as working electrode with lithium metal on the negative electrode side as counter electrode. A battery can be configured by combining two half-cells.

In this study, the half-cells are composed of Li foil (φ: 15 mm, thickness: 0.1 mm) as

a counter electrode, $LiBH_4$ as a solid electrolyte, and the V-LiH mixture material for battery performance test. Firstly, a stainless steel current collector was placed in the pellet maker, and Li metal foil with a diameter of 15 mm was put on it. Thereafter, 50 mg of $LiBH_4$ powder was placed so as to cover the Li metal foil and pressed under 10 MPa for 5 min. Finally, 10 mg of the above-prepared V-LiH mixture material was weighed and placed on a pressed $LiBH_4$ together with the Li foil and stainless steel current collector. In this case, pressurization was carried out under 40 MPa for 5 min. Through these steps, the half-cell used for evaluation was prepared as shown in Figure 3-3. The obtained pellet (Figure 3-4) was sealed in coin type cell. All the procedures were done in glove-box to avoid exposure air.

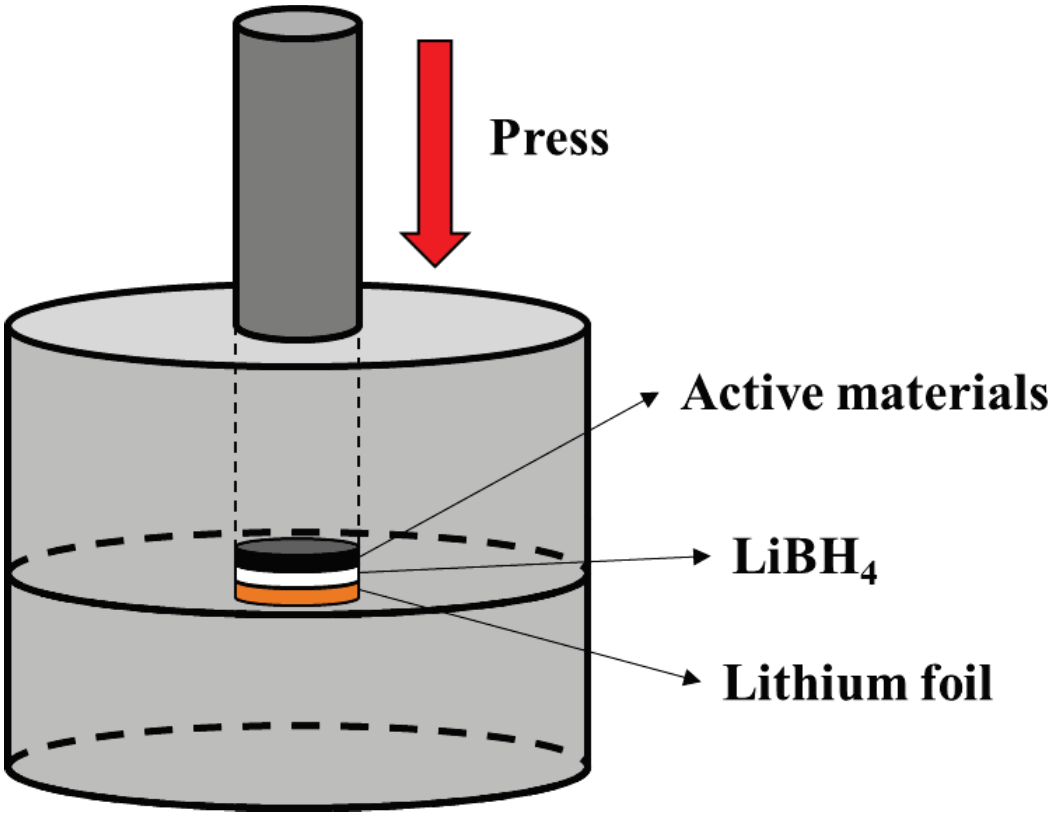

Figure 3-3 Fabrication of all-solid-state lithium-ion-batteries.

Figure 3-4 Practical illustrations of the V-LiH–$LiBH_4$|$LiBH_4$|Li all-solid-state lithium-ion-battery.

3.4 Battery performance

Battery performance has various characteristics. For example, there are charge / discharge capacity characteristics, cycle characteristics, rate characteristics, internal resistance characteristics and so on. The charge / discharge capacity characteristics indicate the amount of power that can be stored in the battery. The cycle characteristics represent the number of times the battery can be used repeatedly. Among these characteristics, the most basic characteristic is the charge / discharge capacity.

Lithium-ion-batteries are generally charged using a constant current and constant voltage charging method. The constant current / constant voltage charging method is called CCCV (Constant Current Constant Voltage) charging method. In the CCCV charging method, charging is performed at a constant current first. Thereafter, when the battery voltage reaches a specified value, charging is performed at a constant voltage. The constant voltage is used to prevent overcharging. The charging ends when the specified time elapses after shifting to constant voltage. During the measurement, the voltage differences between the positive and negative electrodes are recorded as experimental data.

Also, rate (C) is generally used for battery evaluation of lithium ion batteries. The

rate means the speed of charging and discharging. For CCCV charging method, 1C is defined as the magnitude of the current that fully charges (or discharges) the theoretical capacity of the battery in one hour. For example, 2C is equivalent to a current value that is twice that of 1C, meaning that the theoretical capacity is completely discharged in 30 minutes.

The charge / discharge capacity of a lithium-ion-battery depends on the materials that make up the battery. The amount of Li ions that can be reacted depends on the material. Therefore, the target response proceeds completely and the total output obtained is called the theoretical capacity. The theoretical capacity is calculated as follows,

$$Q_{theoretical} = \frac{F \times n}{M} \quad (3\text{-}1),$$

where F is the Faraday constant (ca. 96500 C/mol or As/mol), n is the mole of electrons of the target charge-discharge reaction and M is the formula weight of active material (g/mol) in the target reaction.

The test cell has a sealed structure, thereby the samples in interior of the cell do not contact with air. Then, charge and discharge properties were investigated by electrochemical test apparatus (HJ1001SD8, Hokuto Denko Co.). For the electrochemical

measurements, voltage window was fixed to 0.005−1.0 **V**, and current density was kept as 10 mA/g (0.05 C). The battery tests were carried out at 125 °C of cell temperature in oil bath because $LiBH_4$ as the solid electrolyte behaves a superior ionic conductivity at this temperature. A schematic of the equipment used is shown in Figure 3-5.

Charge and discharge tests were performed, and the capacity was estimated from the results as follows. The profile shown in Figure 3-6 was obtained by this measurement. The voltage time diagram obtained from this measurement is called the "charge / discharge curves". Capacity can be calculated from this charge / discharge curve. Firstly, the electrochemical potentials of both electrodes before charge and discharge tests are measured, in which the measured potential should be corresponding to the voltage compared with the metallic lithium voltage denoted as the unit of **V in Li^+/Li**. The voltage of Li metal is about −3 **V** compared with hydrogen standard voltage. In the case of Figure 3-6, the cell voltage before measurement is about 0.5 **V**. The constant current is applied to decrease (or increase) the voltage from this state. In general, the process of increasing cell voltage is defined as discharge, and the process of decreasing cell voltage is defined as charge. This is because lithium is in the most stable metal state thermodynamically, so the reaction of $Li^+ + e^- \rightarrow Li$ proceeds and the cell voltage becomes 0 **V**. In other words, the movement of lithium ions is important.

When it reaches a certain voltage, it shifts to the equilibrium process corresponding to the electrochemical reaction. In the case of Figure 3-6, it means about 1.0**V**. Cell voltage maintaining constantly until the target electrochemical reaction is complete. During this time, electrons continue to flow. When the target reaction ends, the voltage decreases (or increases) again. If the next reaction voltage is reached, a constant voltage is maintained until the target electrochemical reaction is completed, and electrons flow during that time. Finally, when the set lower limit voltage (or upper limit voltage) is reached, the discharging (or charging) process ends. From the obtained charge and discharge curves, the specific capacity as a unit mAh/g of the electrode materials is calculated as follows,

$$Q = \frac{i \times t}{w} \qquad (3\text{-}2),$$

where i is the applied constant current (mA), t is the time of charge-discharge (h) and w is the weight of active material (g).

In general, there are two types of measuring cells, which are two-electrode and three-electrode types. This study used the two-electrode type measuring cell to study the electrode characteristics of all-solid-state lithium-ion-batteries.

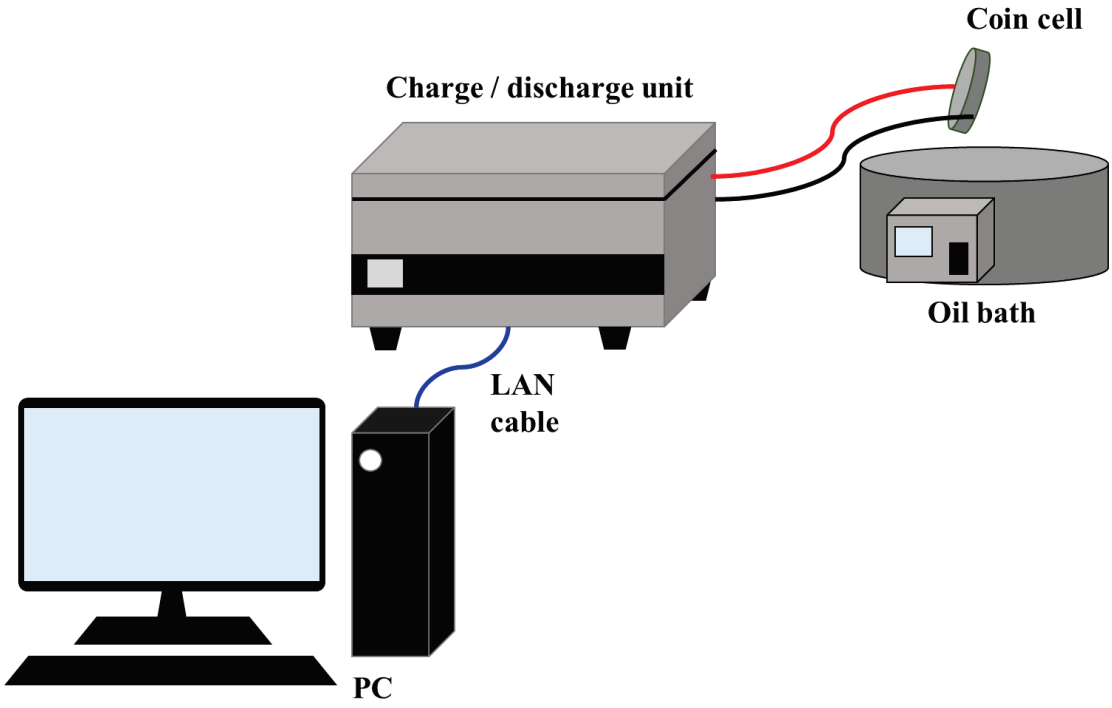

Figure 3-5 Schematic of charge and discharge measurement device.

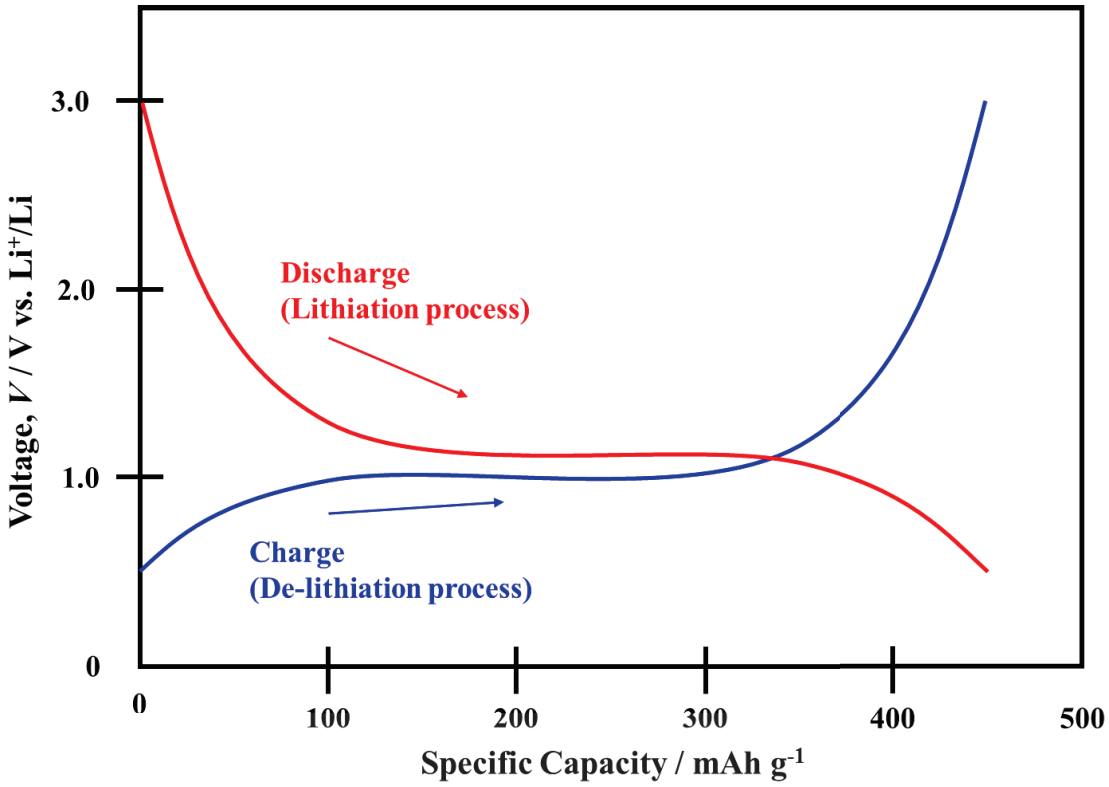

Figure 3-6 Schematic of charge and discharge curves. The red line shows the discharging process and the blue line shows the charging process. In the discharge process, lithium ions receive electrons.

3.5 Characterization techniques

3.5.1 Powder X-ray diffraction (XRD) measurements

X-ray diffraction (XRD) is a technique to identify crystal phase of compounds. Figure 3-7 shows a schematic image of X-ray diffraction for the crystal. Incident X-rays to the crystal are scattered by atoms in the crystal, but as a result of interference of scattered X-rays, it becomes strong in a specific direction satisfying certain conditions. Since the conditions are determined by the crystal structure, information on the crystal structure can be obtained by analyzing the X-ray diffraction profile. As shown in Equation 3-3, when monochromatic X-rays with wavelength λ are radiated to a crystal face of lattice spacing d at an angle θ satisfying the Bragg's equation, the X-rays scattered at an angle of 2θ with respect to the incident beam direction have the same phases in both the scattered X-rays, and they are strengthened and diffracted X-rays are obtained.

$$n\lambda = 2\mathrm{d}_{hkl} \sin\theta \ (n = 1, 2, \dots) \qquad (3\text{-}3)$$

($*$ hkl are Miller indices)

Since the angle 2θ formed by the incident X-ray and the diffracted X-ray varies depending

on the spacing between the lattice planes, an X-ray diffraction profile can be obtained by detecting X-rays during continuously varying 2θ. Therefore, by analyzing this profile, the crystal structure can be determined. In addition, by analyzing the diffraction peaks, the crystallite size can be estimated as well.

In this work, to investigate structural change of the electrode material, Powder X-ray diffraction (XRD) measurements were performed by using Cu-Kα (λ=0.154 nm) radiation at room temperature (RINT-2500V, Rigaku Co.). The conditions to generate X-rays were 40 kV as the accelerating voltage and 200 mA as the tube current. The measurement sample was spread and fixed on the glass plate with high vacuum grease (APIEZON®, H type, M&I Materials Ltd.) and was sealed with a polyimide sheet (Kapton®, DuPont-Toray Co., LTD,) in a glove-box to prevent degradation due to oxidation of the sample. After each charge and discharge step, XRD measurement was carried out by a method of extracting a sample from a cell (Ex-situ XRD). The obtained XRD patterns were analyzed by using the PDXL software (version 1.7.0.0, Rigaku Co.) with powder diffractions files (PDF) in the database.

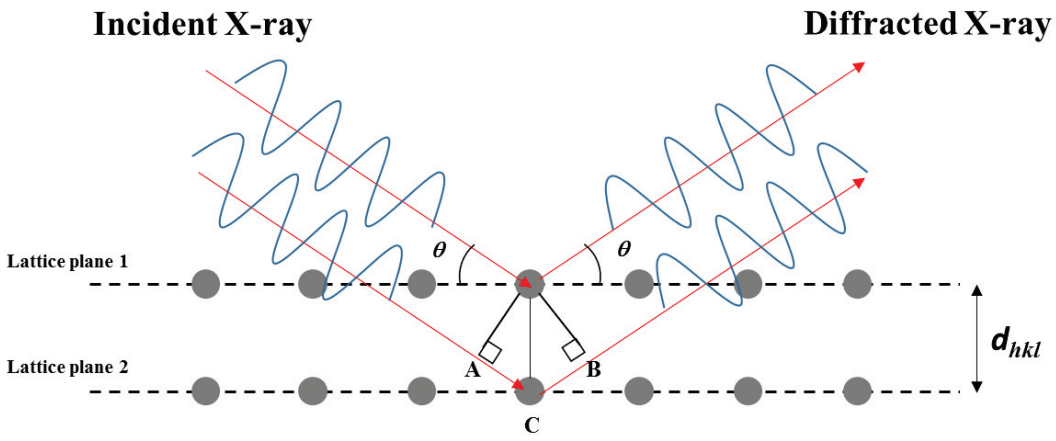

Figure 3-7 Diffraction of X-ray from lattice planes in crystal [3-2].

3.5.2 Quantitative analysis using gas chromatography

Gas chromatography is a method that can separate and detect a sample gas and perform qualitative and quantitative determinations of the gas composition. Explanation of the mechanism of separation in gas chromatography is indicated as follows (Figure 3-8). The gaseous sample is introduced into the device and is carried into the column by the carrier gas (He, N_2 or Ar). In the column, the interaction (adsorption, distribution) between the sample component and adsorbent in the column selectively is different for each component. As a result, a difference appears in the detection time. Since the detector converts the amount of each component into an electric signal and sends a signal to the data processing device, the qualitative and quantitative analyses of components in the sample gas can be achieved.

There are various detection methods. The principle of the thermal conductivity detector (TCD) used in this experiment is explained below. TCD is a nondestructive detector that detects the difference in thermal conductivity between a compound and a carrier gas. The principle is that in the Wheatstone bridge circuit as follow in Figure 3-9, the analysis gas (carrier gas and sample component) and reference gas from the separation column pass through the R_1 and R_3 filaments, respectively. Apply current to the filament

and balance the bridge (0 **V** response to G). When the carrier gas passes through the filament, heat is dissipated by heat conduction. With carrier gas alone, the temperature is kept constant. When the target compound is contained, the thermal conductivity of the gas changes. The filament temperature changes. As a result, the resistance value also changes, causing the bridge to lose balance and generating a voltage at G. This is led to the recording unit. For devices controlled to keep the filament temperature constant, measure and record the current required to restore the filament temperature from changes in its resistance value.

In this study, gas analysis during charge process inside the battery cell was carried out. While measuring charge, in order to measure the pressure change in the cell due to gas generation, a special battery cell was fabricated in which a SUS tube was attached to the upper part of the battery cell as shown in Figures 3-10 and 3-11. Gas generated in the charge process was transferred to gas chromatography (SHIMADZU, GC-14B) while filling the special battery cell with gas, and gas chromatography analysis was carried out. Packed Colum (Shinwa Chemical Industries Ltd., SHINCARBON ST, 2.0 m × 3.0 mm) was used to separate the generated gases.

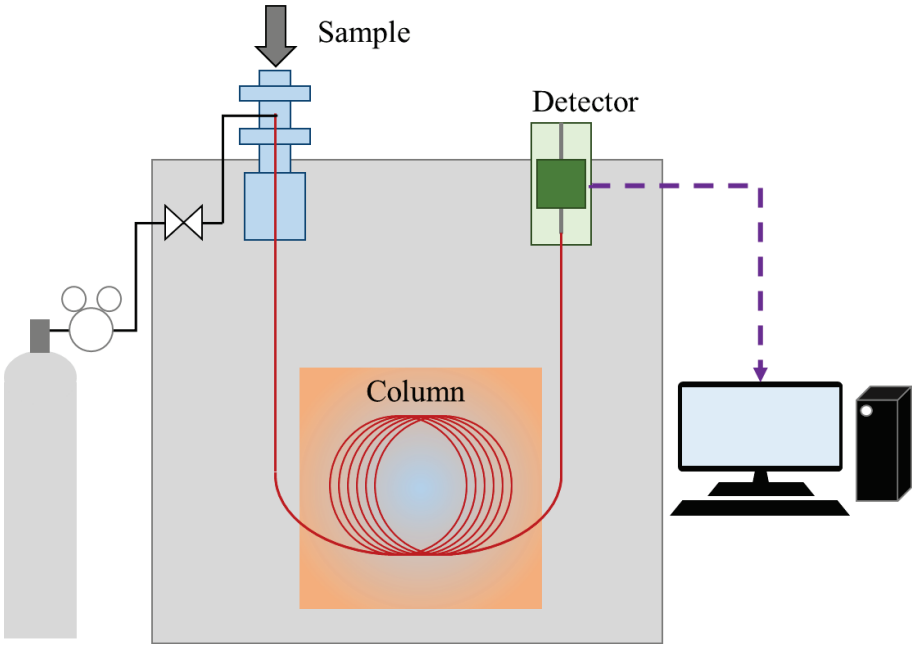

Figure 3-8 Schematic view of gas chromatography [3-3]. Each component is detected separately because the time between the sample introduction into the instrument and the appearance of the peak varies for each component.

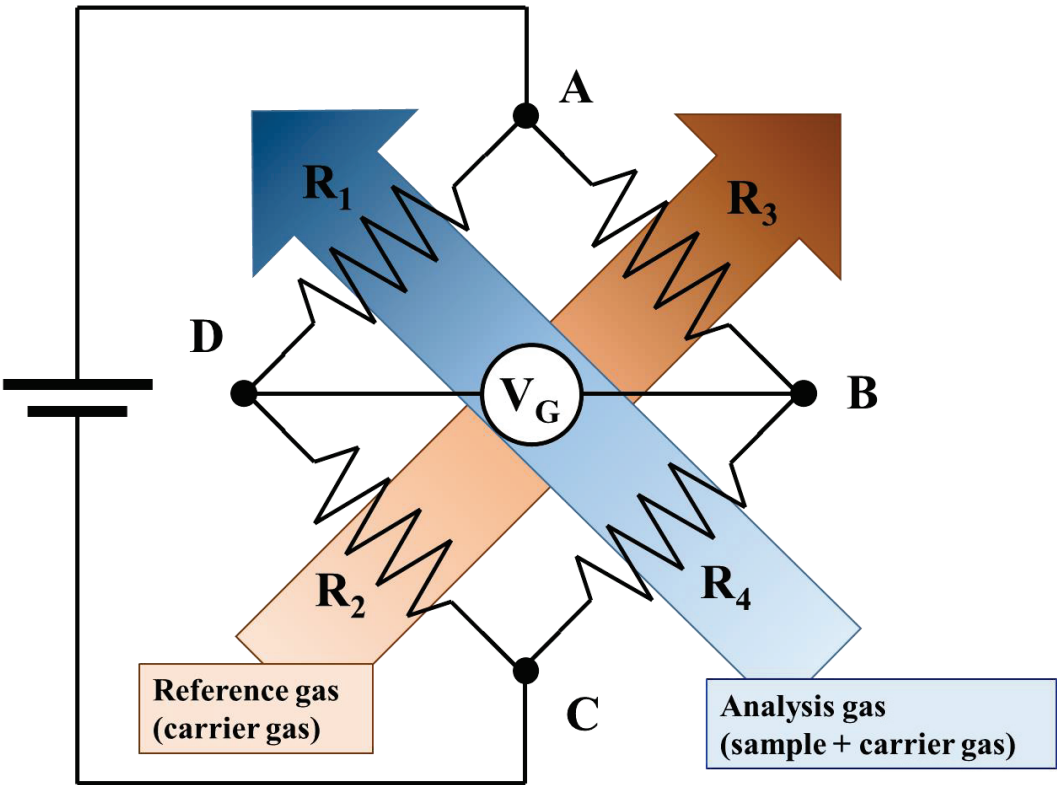

Figure 3-9 Wheatstone bridge circuit. When the analysis gas flows, the temperature of the filament changes. As a result, the change in the voltage between C and D is read as a signal.

Figure 3-10 Special cell for gas analysis.

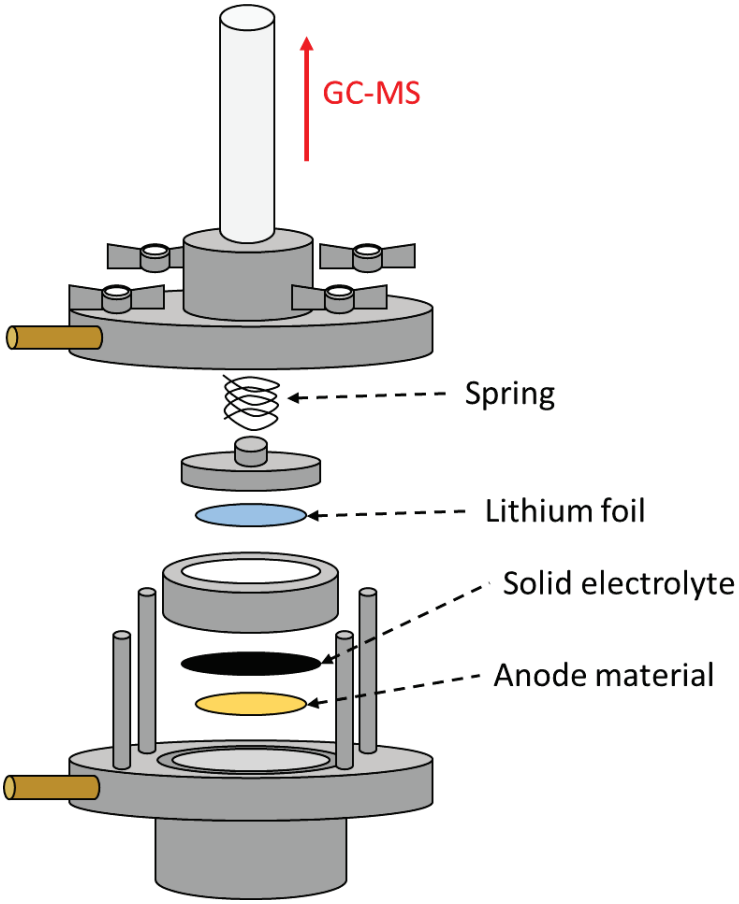

Figure 3-11 Schematic picture of an electrochemical cell. A spring mounted inside the battery enhances the contact between the electrode materials and the solid electrolyte.

References

[3-1] J. J. Reilly and R. H. Wiswall: *Inorganic Chemistry* 9 (1970) 1678–1682.

[3-2] I. Nakai and F. Izumi: *X-ray Powder Analysis (Rietveld refinement)*: Asakura Publishing (2002) (Japanese).

[3-3]

https://www.an.shimadzu.co.jp/gc/support/faq/fundamentals/gas_chromatography.htm

4 Results and discussion

4.1 Synthesis of V-LiH mixture material using milling process

As mentioned in the chapter 2, VH_2 is unstable hydrogenated state at 40 °C under ambient pressure of H_2. Therefore, in this study, electrode material was prepared from V and LiH as a starting material using milling process.

Figure 4-1 shows the XRD profile of the V-LiH mixture material after the ball-milling. The profile labeled “Milled V + LiH” is a profile after the initial milling of V and LiH. From the XRD database [4-1, 4-2], the observed peaks were mainly assigned to V and LiH as starting materials. However, the diffraction peaks not attributed to V and LiH were observed around $2\theta = 40$ °. From the XRD database [4-3, 4-4], it was suggested that the diffraction peak is corresponding to $VH_{(0.5+x)}$ (x: 0 ~ 0.5).

Electrode material composed of V-LiH mixture, acetylene black, and $LiBH_4$, was examined by XRD, indicated that the diffraction peaks of V and LiH in the starting material decreased after the milling process. However, the diffraction peak indicating $VH_{(0.5+x)}$ increased. From the XRD database [4-3, 4-4, 4-5], the XRD measurements of this electrode composite revealed that the composition was close to that of $VH_{0.81}$ (when $x = 0.31$).This phenomenon indicates that a reaction of $V + 0.81LiH \rightarrow VH_{0.81} + 0.81Li$

partially proceeds as a mechano-chemical reaction during mechanical ball-milling process before the electrochemical test.

4.2 Anode characteristics of all-solid-state lithium-ion-batteries using V-LiH electrode material

Figure 4-2 shows charge / discharge profiles of the V-LiH electrode for the 5 cycles. The horizontal axis shows the capacity per VH_2 weight. The charging reaction with increase in the potential to 1.0 **V** was indicated as "De-lithiation process" and the discharging reaction with decrease in the potential to 0.005 **V** was indicated as "Lithitation process" at a current density of 10 mA/g at a cell temperature of 125 °C. The theoretical conversion reaction is expressed by the following equations.

$$\text{De-lithiation process : } V + 2LiH \rightarrow VH_2 + 2Li^+ + 2e^- \quad (4\text{-}1)$$

$$\text{Lithiation process : } VH_2 + 2Li^+ + 2e^- \rightarrow V + 2LiH \quad (4\text{-}2)$$

The theoretical charge/discharge capacity is 1013 mAh/g. The charging properties of 1st cycle are examined at first. As is shown in Figure 4-3, the charging process of 1st cycle is only started from 0.53 **V**. As mentioned above, this is due to the formation of $VH_{0.81}$ during the mechanical ball milling process. When increasing the voltage with a constant

current, the equilibrium potential was confirmed around 0.65 **V**. From the following Nernst' equation, the theoretical reaction potential of equations (4-1) and (4-2) was calculated to be about 0.72 **V** to form VH_2, where the thermodynamic quantities are shown in Table 4-1 obtained from the database [4-6, 4-7].

$$E = (1/xF)\,[\Delta H(VH_x) - T(\Delta S(VH_x) - \Delta S(V)) + xT(\Delta S(LiH) - \Delta S(Li)) - x\Delta H(LiH)] \tag{4-3}$$

$$= -\{\Delta_f G°(2LiH+V) - \Delta_f G°(VH_2+2Li)\}/2F \tag{4-4}$$

In the 1st cycle charging, the capacity of about 1069 mAh/g was obtained. The capacity obtained is smaller than the theoretical capacity of 1013 mAh/g. In the case of the theoretical formula, the starting materials are V and LiH. However, in this study, it was estimated that the capacity was small because a small amount of $VH_{0.81} \approx VH_{(0.5+x)}$ (x: 0 ~ 0.5) was included at the start of the measurement. Compared with the theoretical potential estimated from thermodynamic data, the electrochemical reaction in the first charge process is corresponding to the conversion reaction to generate VH_2 in the plateau

region (0.65 **V**). The plateau voltage around 0.65 **V** for the 1st charging should be corresponding to the following equation.

$$VH_{0.81} + 1.19LiH \rightarrow VH_2 + 1.19Li^+ + 1.19e^- \qquad (4\text{-}5)$$

However, the amount of 1.19Li has only ca. 600 mAh/g capacity. The capacity of 600 mAh/g obtained for the 1st charging is corresponding to the length of plateau, which is much smaller than that of total capacity of 1069 mAh/g. The extra 469 mAh/g suggests that lithiation / de-lithiation properties similar to the previously reported hard carbon (non-graphitizable carbon) were obtained. This is probably because Li atoms that did not react with V during ball milling processes for electrode production reacted with acetylene black mixed as a conductive material and changed into a state similar to that of lithiated hard carbon.

Then, the electrochemical reaction for the 1st charging process shows a conversion process to generate VH_2 for the plateau region and a hard-carbon-like delithiation process for the slope region.

However, as shown in Figure 4-4 corresponding to 1.0 **V**, the generated product is $VH_{0.81}$ although the expected product should be VH_2, indicating that the generated product does not change even after charging process with 600 mAh/g capacity. However, as mentioned above, VH_2 is unstable without H_2 pressure. The generated VH_2 must be decomposed to incomplete hydride phase $VH_{0.81} \approx VH_{(0.5+x)}$ (x: 0 ~ 0.5) with slightly high stability during the XRD measurement.

Next, the discharging properties of 1st cycle were examined. With respect to the 1st discharging process, about 1226 mAh/g capacity in total is shown with a prompt slope (1-0.6 **V**; ca. 50 mAh/g), a first plateau (0.6-0.45 **V**; ca. 700 mAh/g), and the other slope (0.44-0.005 **V**; ca. 420 mAh/g), indicating that the total capacity is larger than 1013 mAh/g corresponding to reaction (4-2). Because the expected coulombic efficiency corresponding to VH_2 conversion reaction cannot be reached to 100%, this total capacity of 1226 mAh/g should contain not only conversion process but also lithiation process to acetylene black (hard-carbon-like). Of course, V single phase was confirmed in the 0.005 **V** and 0.3 **V** XRD profiles of Figure 4-5. It is suggested that the conversion reaction in which $VH_{0.81}$ becomes V and LiH occurs reversibly in the initial charge and discharge

process. From the above results, it is suggested that the conversion reaction of V and LiH in 1st cycle may proceed in the following two stages [4-8, 4-9, 4-10, 4-11, 4-12].

$$VH_{0.81} + 1.19LiH \Leftrightarrow VH_2 + 1.19Li^+ + 1.19e^- \quad (4\text{-}5)$$

$$VH_2 + 2Li^+ + 2e^- \Leftrightarrow V + 2LiH \quad (4\text{-}6)$$

Here, focusing on the 2nd to 5th discharging cycles, the discharge profiles are very similar. It is presumed that the same electrochemical reaction has occurred after the 2nd cycle. In particular, the profiles corresponding to more than 0.6 **V** and less than 0.3 **V** are quite similar. Focusing on the region exceeding 0.6 **V** and less than 0.3 **V**, it is clear that the capacity has not changed drastically with the increase of the cycle. Therefore, these region is assumed to be the contribution of lithiation to acetylene black (hard-carbon-like) (470 mAh/g) even after the 2nd cycle. The rest should correspond to the conversion reaction. The capacities obtained in each charge and discharge cycle are summarized in Table 4-2.

We assumed that the contribution of lithiation to acetylene black (hard-carbon-like) is 470 mAh/g and this value doesn't drastically change with the increasing cycles. The remaining part should be corresponding to conversion reaction. Figure 4-6 shows the discharging profiles of each cycle, which are subtracted by the expected lithiation profile corresponding to acetylene black (hard-carbon-like) shown in the inset of Figure 4-6. As shown in Figure 4-6, three plateaus are clearly recognized in the early stages of cycles. And the lengths of the low plateaus around 0.34-0.4 **V** shown by horizontal arrows do not change with the increasing cycles, indicating about 150 mAh/g. However, the lengths corresponding to the high voltage region shown by vertical arrows are decreased drastically from 600 to 50 mAh/g for the 1st cycle and 5th cycle, respectively. In particular, the high plateau voltage, indicated by the vertical arrow, and the low plateau voltage, indicated by the dashed line, decrease with increasing cycles. However, the intermediate plateau voltage around 0.45 **V** is maintained as the cycle increased. Although this has not yet been fully elucidated, it was guessed that the β phase change occurred at this intermediate plateau voltage of 0.45**V**. As the discharging processes included not only the conversion reaction of V-LiH to VH_2 but also the lithiation reaction of acetylene black (hard-carbon-like), the charging processes after 2nd cycle should include the de-lithiation reaction with 470 mAh/g capacity.

Again, focusing on the 2nd cycle charging profile shown in Figure 4-2, the slope regions below 0.45 **V** (130 mAh/g) and above 0.65 **V** (90 mAh/g) show about 220 mAh/g total capacity, indicating that remaining capacity of 250 mAh/g should be hidden in the plateau regions between 0.45 and 0.65 **V**.

Therefore, the remaining capacities of ca. 250 mAh/g corresponding to 0.45 **V** plateau and of ca. 600 mAh/g corresponding to 0.65 **V** plateau can be explained by the conversion reactions of $V + 0.81LiH \rightarrow VH_{0.81} + 0.81Li$ and $VH_{0.81} + 1.19LiH \rightarrow VH_2 + 1.19Li$, respectively. And, with increasing cycles, the charging processes are reproduced well to have about 900 mAh/g capacity in the total of conversion and lithiation reactions. Of course, the capacities corresponding to higher plateau region around 0.65 **V** for the charging show the slightly decreased phenomena, indicating a good agreement with the decreasing trend of higher plateau region capacity of the 2nd to 5th discharging processes.

Finally, the capacity corresponding to the lithiation / de-lithiation reaction of acetylene black (hard-carbon-like) is discussed. The capacity of 470 mAh/g was calculated due to the gravimetric amount of VH_2. Therefore, the capacity calculated from the amount of carbon should be different. Actually, the amount of acetylene black is 30/40 ratio compared with the amount of V + 3LiH. Because the total weight corresponding to

V + 3LiH is 75, the corresponding VH_2 and carbon amounts should be 53 and 56, respectively. Therefore, 470 mAh/g capacity due to the VH_2 weight should be converted to 444 mAh/g due to the carbon weight, indicating this value is quite reasonable as is assumed by lithiation of hard carbon [4-13].

Table 4-1 Thermodynamic properties of vanadium hydride [4-6, 4-7].

Materials	$\Delta_f H°$ (kJ/mol)	$\Delta S°$ (J/mol)	$\Delta_f G°$ (kJ/mol)
V-VH_2	–40.2	–142.2	2.20
Li-LiH	–90.63	–74.06	–68.55

Table 4-2 The capacities obtained in each charge and discharge cycle.

	Specific Capacity [mAh g^{-1}]				
	1st	2nd	3rd	4th	5th
De-lithiation process (0.005 **V** → 1.0 **V**)	1069	1047	835	733	681
Lithiation process (1.0 **V** → 0.005 **V**)	1226	917	777	709	674

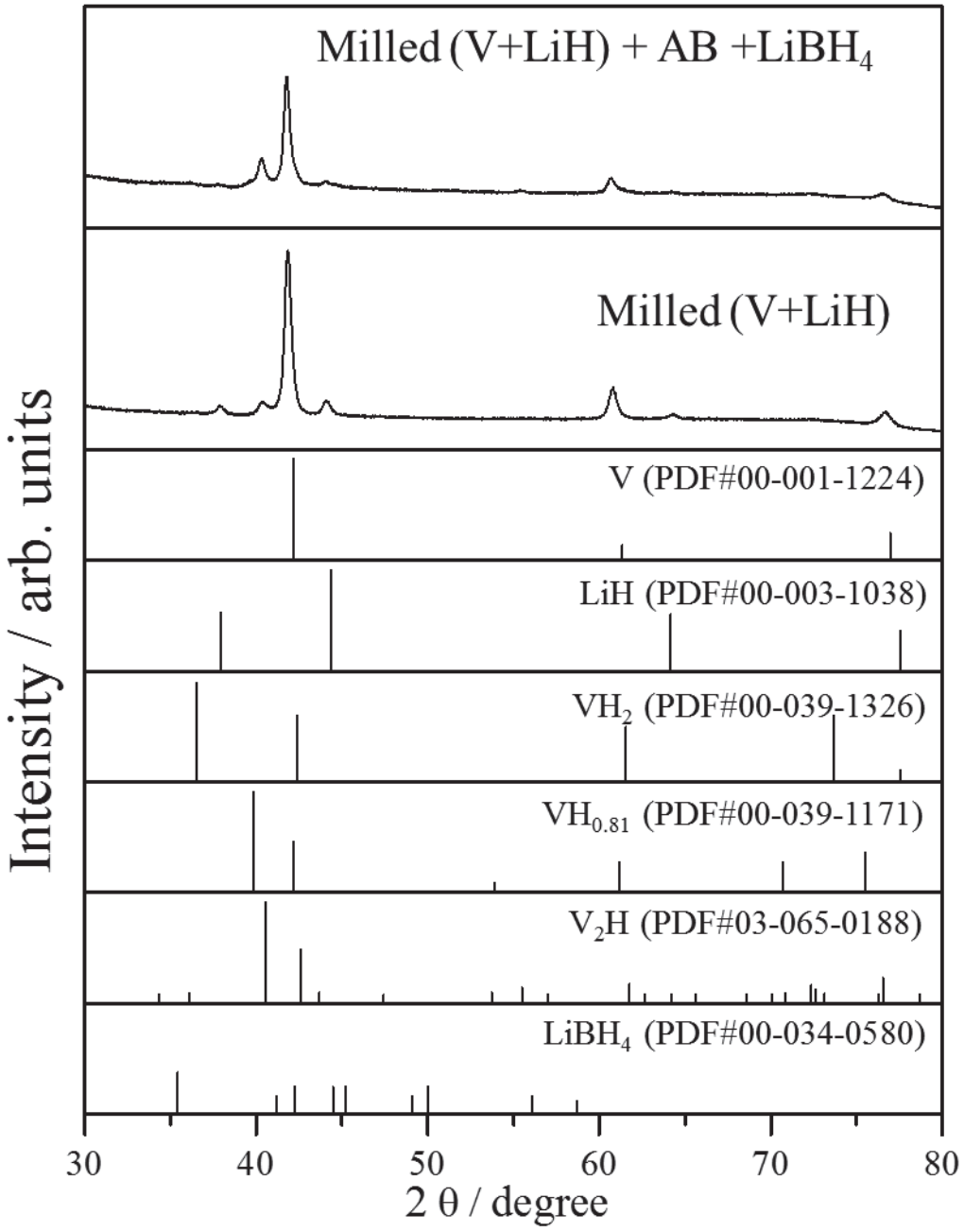

Figure 4-1 Ex-situ XRD patterns of V-LiH electrode at 1st and 2nd milling process. The bottom panels show the XRD peak positions corresponding to the different phases from the PDXL database.

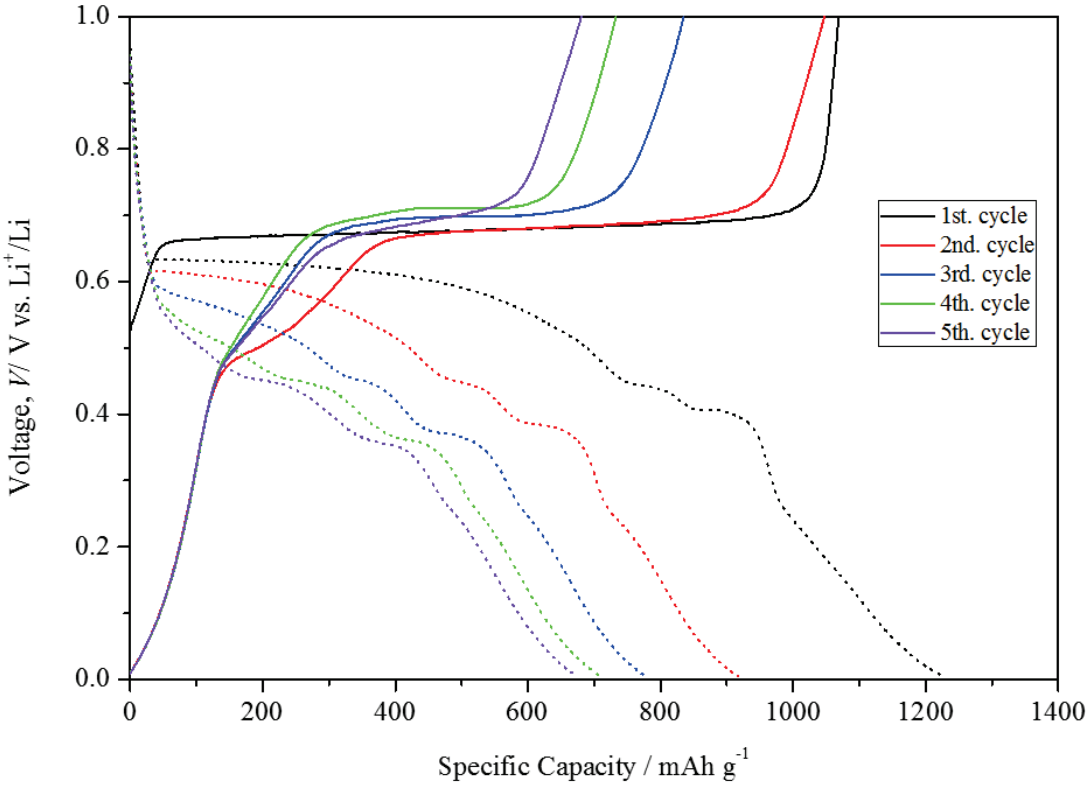

Figure 4-2 Cyclic performances of the V-LiH electrode in the voltage range of 0.004-1.0 **V** at 125 °C of cell temperature. A Current density was kept as 10 mA/g (0.05 C). The horizontal axis shows the capacity per VH_2 weight.

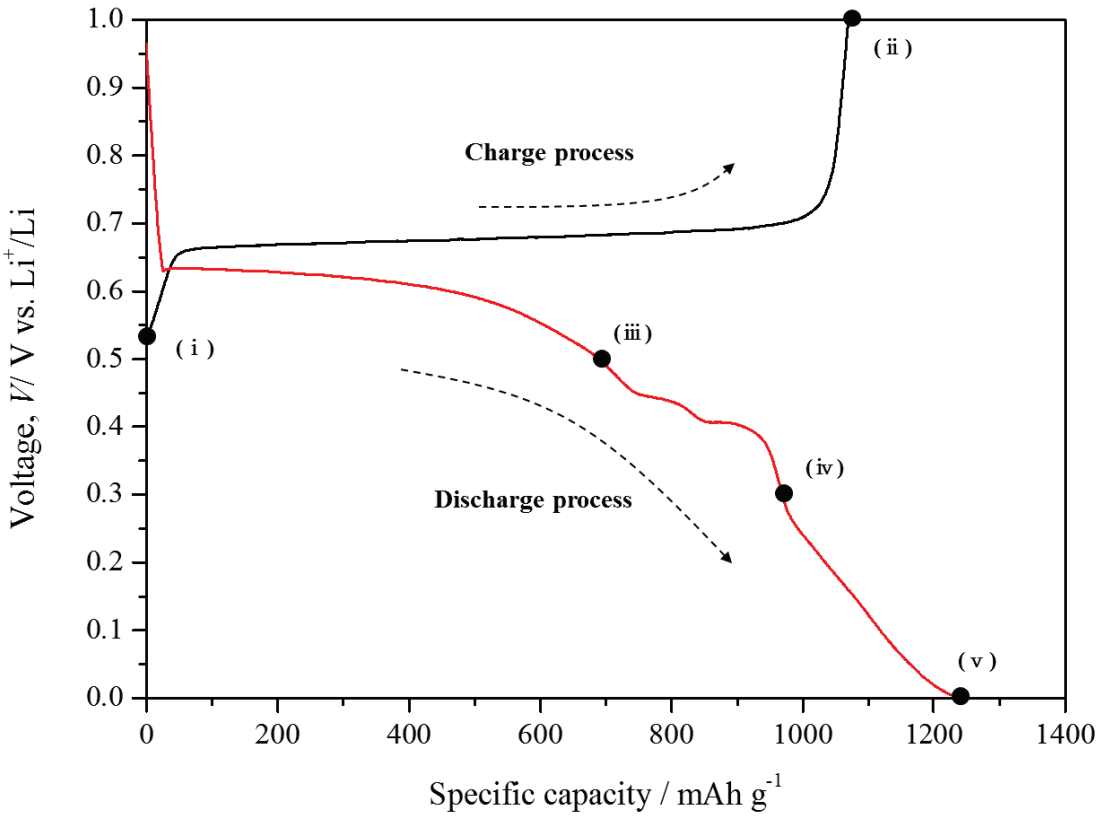

Figure 4-3 First Galvanostatic charge-discharge curves for V-LiH electrode in the voltage range of 0.004-1.0 **V** at 125 °C of cell temperature. The roman numbers, (i), (ii), (iii), (iv), and (v) in the figure, indicate the reaction steps, respectively. (i) shows the measurement start time, (ii) shows the end of the charge process, (iii) and (iv) indicate the middle of the discharge process, and (v) shows the end point of discharge. In each of these charge and discharge steps, the battery cell was disassembled and XRD measurement was carried out.

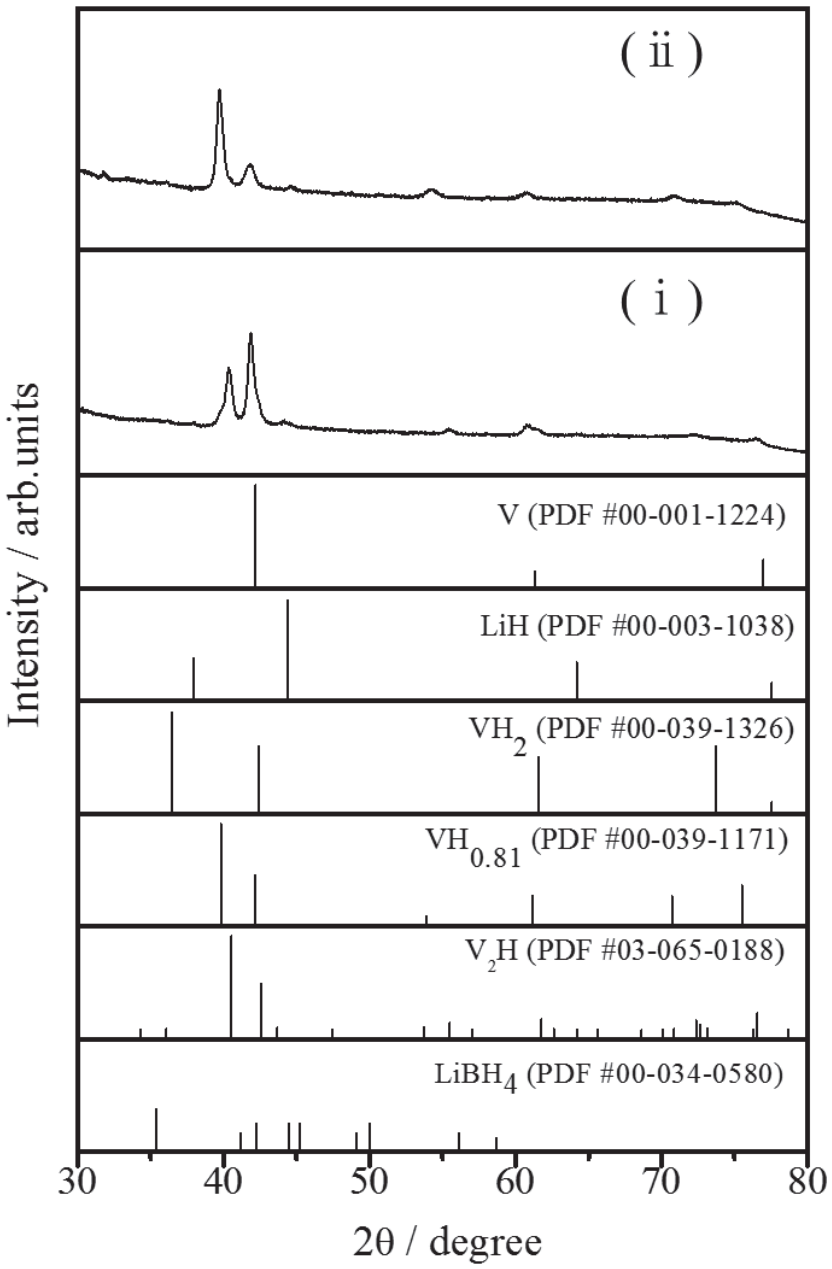

Figure 4-4 Ex-situ XRD patterns of V-LiH electrode during charge process between 0.6 **V** and 1.0 **V**. (i) shows the measurement start time at 0.6 **V**, (ii) shows the end of the charge process at 1.0 **V**.

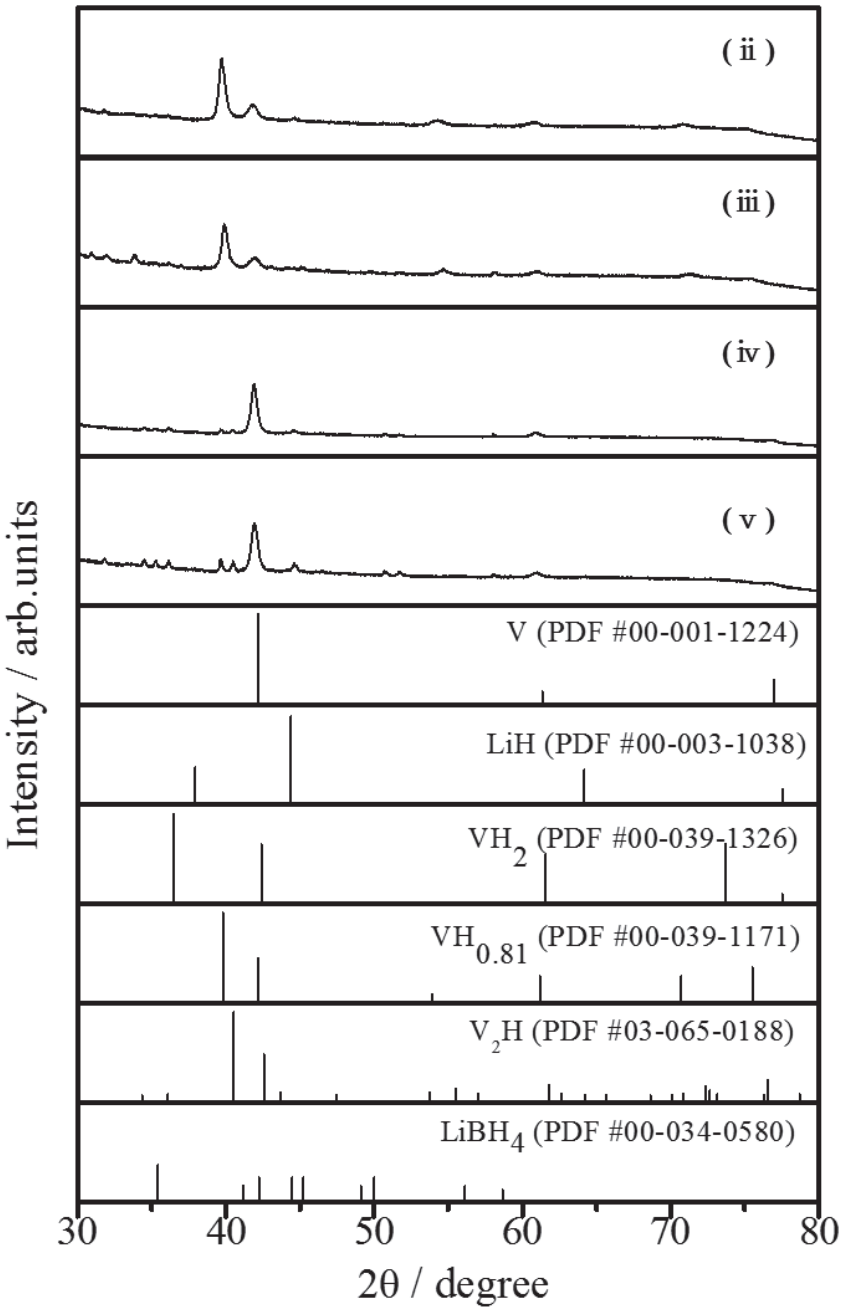

Figure 4-5 Ex-situ XRD patterns of V-LiH electrode during discharge process from 1.0V to 0.005 **V**. (iii) and (iv) indicate the middle of the discharge process at 0.5 and 0.3 **V**, and (v) shows the end point of discharge at 0.005 **V**.

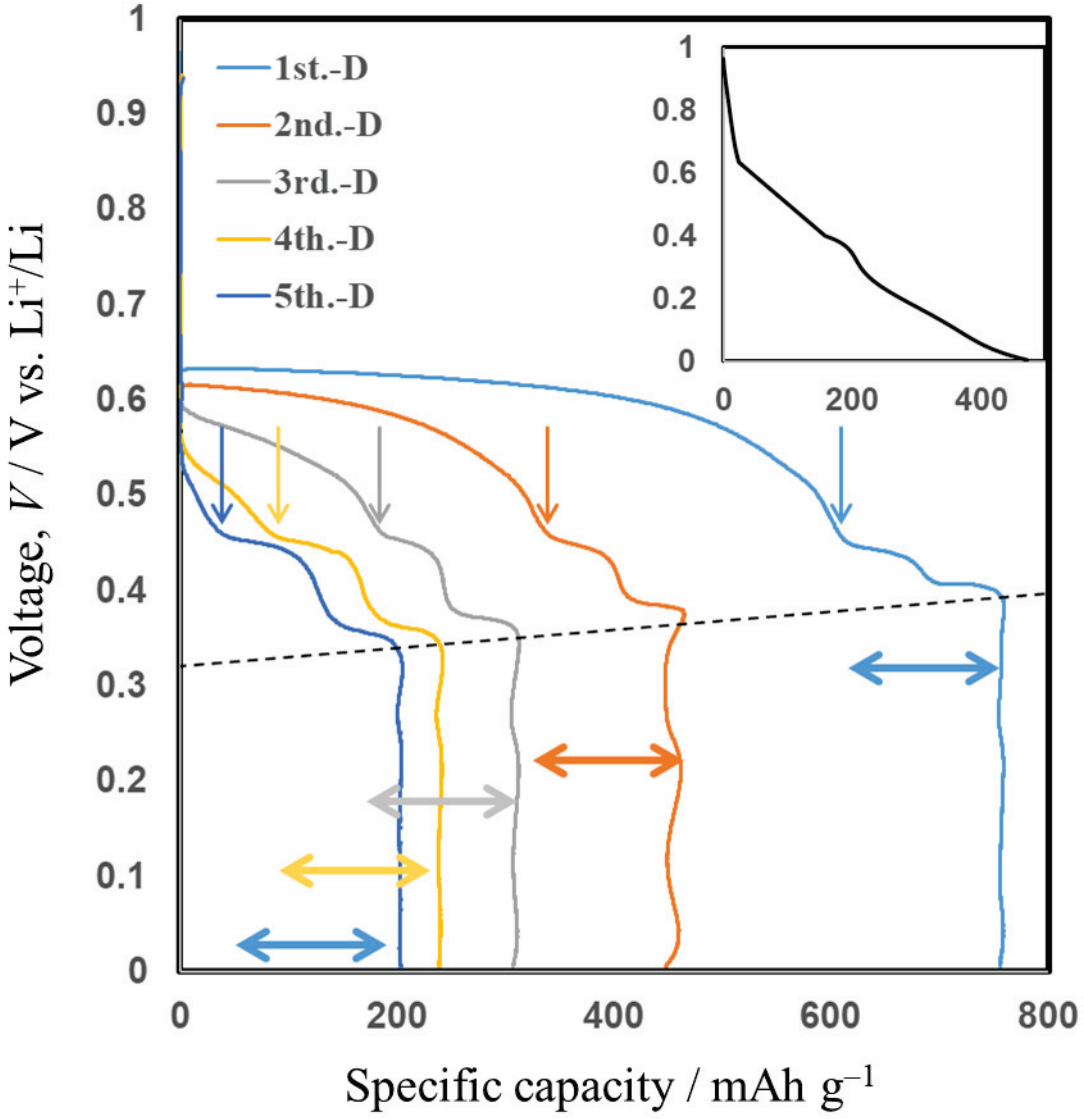

Figure 4-6 Discharging curves subtracted by the assumed profile of hard carbon shown in the inset. Vertical arrows show the end points corresponding to higher plateaus regions and horizontal arrows show remaining capacities of each profile.

4.3 Gas pressure measurement

The conversion reaction process and cycle characteristics were investigated for the V-LiH electrode in Chapters 4.1 ~ 4.2. The reaction potential (0.65 **V**) obtained by charge and discharge measurement is close to the theoretical reaction potential (0.72 **V**) of V and LiH. It was suggested that the conversion reaction may proceed between V and LiH. However, it was not clear from the results of XRD whether VH_2 was formed. Therefore, as a reference experiment, a gas monitor experiment was performed while charging and discharging.

Figure 4-7 shows the relationship between the internal cell pressure up to 1.0 **V** and the initial charge curve. The cell voltage rose to 0.6 **V** simultaneously with the start of the measurement. After that, a large plateau was observed around 0.6 **V**. It indicates the expected conversion reaction of VH_2 generation. The internal pressure of the cell gradually increased as the reaction progressed.

Since the battery cell used for the gas monitor experiment had free space of about 10 cm^3 inside the cell, it was considered that the unstable VH_2 might have released hydrogen. A phenomenon different from the coin cell experiment up to Chapter 4.2 occurred. In the case of the coin cell, VH_2 was formed because the electrochemical potential worked on

the electrode after the reaction was completed. However, it was considered that when the cell was disassembled, the electrochemical potential was released and changed to $VH_{0.81}$.

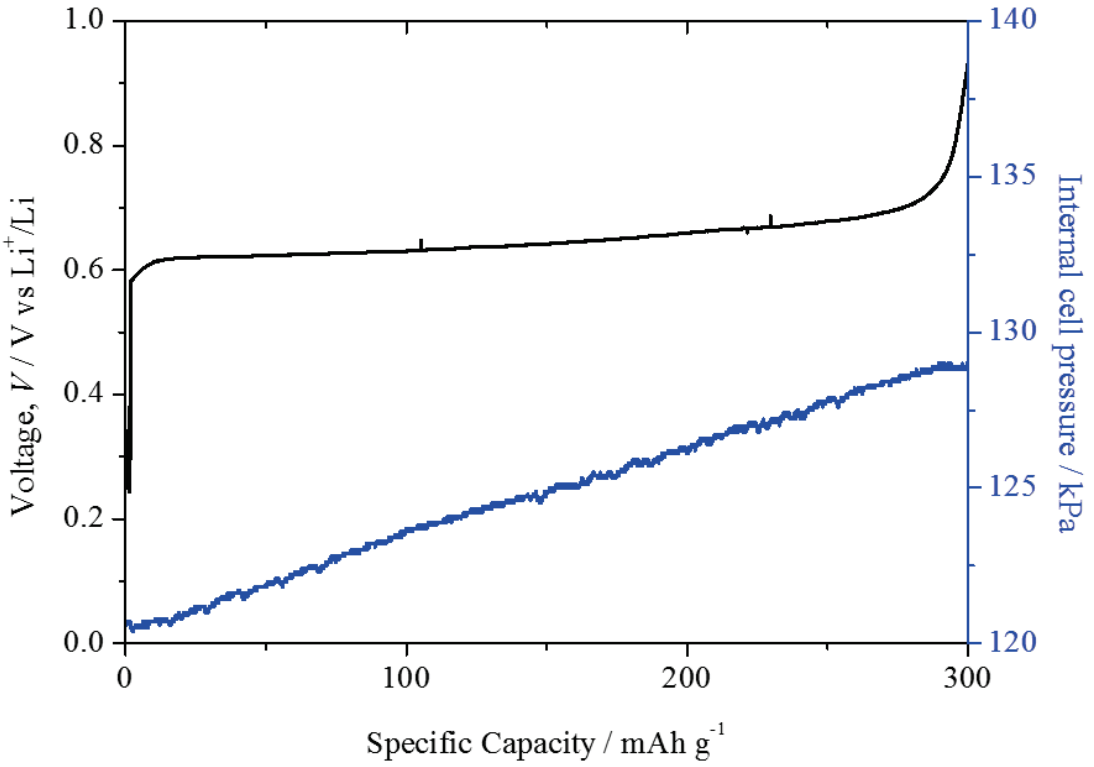

Figure 4-7 Relationship between voltage change and cell internal pressure change during de-lithiation process at 125 °C of cell temperature. The vertical axis on the left shows the cell voltage. The vertical axis on the right shows the internal cell pressure. The horizontal axis shows the capacity per VH_2 weight.

References

[4-1] J.D. Hanawalt, H.W. Rinn and L.K. Frevel: *Industrial and Engineering Chemistry, Analytical Edition* 10 (1938) 475.

[4-2] E. Zintl, A. Harder: *Zeitschrift für Physikalische Chemie* 14 (1931) 264-284.

[4-3] Y.Noda, K.Masumoto, S.Koike, T.Suzuki and S.Sato: *Acta Crystallographica Section B* 42B (1986) 529.

[4-4] H. Müller and K. Weymann: *Journal of the Less Common Metals* 119 (1986) 115-126.

[4-5] C.W.F.T. Pistorius: *Zeitschrift für Physikalische Chemie* 88 (1974) 253–263

[4-6] Y. Ohsumi: *Hydrogen storage alloy*, AGNE Gijutsu Center publishing (1993) (Japanse).

[4-7] Chase, M.W., Jr., NIST-JANAF Themochemical Tables, Fourth Edition, *J. Phys. Chem. Ref. Data, Monograph* 9, 1998, 1-1951.

[4-8] T. Namba, H. Ezaki, M. Takagi, H. Yukawa and M. Morinaga: *Journal of Alloys and Compounds* 330-332 (2002) 318–322.

[4-9] H. Yukawa, D. Yamashita, S. Ito, M. Morinaga and S. Yamaguchi: *Materials Transactions* 43 (2002) 2757-2762.

[4-10] R. Kawai, H. Yukawa, A. Suzuki, T. Namba and Y. Murata: *International Journal of Hydrogen Energy* 42 (2017) 22564-22574.

[4-11] S. Kumar, G.P. Tiwari and N. Krishnamurthy: *Journal of Alloys and Compounds* 645 (2015) S252–S256.

[4-12] S. Kumar, A. Jain, T. Ichikawa, Y. Kojima and G.K. Dey: *Renewable and Sustainable Energy Reviews* 72 (2017) 791–800.

[4-13] V.G. Khomenko and V.Z. Barsukov: *Electrochimica Acta* 52 (2007) 2829-2840.

5. Conclusion

In this study, we aimed to elucidate new electrochemical properties as electrode materials for lithium-ion-batteries based on the hydrogen storage/release characteristics in the vanadium system which has been reported so far.

This study has shown that reversible electrochemical reactions can proceed with relatively thermodynamically unstable substances such as vanadium hydride. As a result, we clarified for the first time that it can be used as an electrode material for lithium-ion-batteries that can achieve an initial charge / discharge capacity exceeding 1000 mAh/g or more.

As a result of the electrochemical performance, the initial states of V and LiH should be partially converted to $VH_{0.81}$ during initial mixing by mechanical ball-milling. Of course, the by-product Li should be reacted with acetylene black, generating the lithiated hard carbon. Therefore, the 1st charging process shows slightly high capacity even though the capacity is decreased with increasing cycles. The 1st charging plateau at 0.65 **V** should be explained by the following conversion reaction, $VH_{0.81} + 1.19LiH \rightarrow VH_2 + 1.19Li$.

In the over all charging / discharging processes, the stable and extra capacity of 470 mAh/g is included as de-lithiation / lithiation processes, respectively. For the discharging

processes after subtracted by hard carbon contribution, three plateaus are obtained. Although the corresponding reaction to each conversion reaction are not clear, high plateau region shown between 0.5 and 0.6 **V** should be explained by the opposite reaction mentioned above, in which the capacity is drastically decreased with increasing cycles. On the other hand, the capacity corresponding to middle and low plateau regions shown around 0.4 **V** is not changed with even increasing cycles.

Finally, in the charging processes, the plateaus of 0.45 ~ 0.53 **V** and 0.65 **V** are, respectively, corresponding to the conversion reactions to generate $VH_{0.81}$ and VH_2, and as extra capacity corresponding to the slope regions of charging process, the de-lithiation reaction proceeded.

6. Acknowledgement

I would like to express my gratitude to my supervisor Prof. Dr. Takayuki Ichikawa for his insightful comments, suggestions and encouragements throughout the course of this study.

I would like to express my special thanks to Prof. Dr. Toshikazu Ekino for his valuable suggestions and discussions.

I would like to show my great appreciation to Associate Prof. Dr. Hiroki Miyaoka for his constructive comments and warm encouragement in my doctoral course life.

I would like to thank to Associate Prof. Dr. Ankur Jain and Prof. Dr. Yoshitsugu Kojima for a lot of valuable suggestion and discussion in my doctoral course life.

I would like to express my sincere thanks to the colleagues of Prof. Kojima's and Prof. Ichikawa's Laboratory, Dr. Keita Nakajima, Dr. Hiroki Uesato, Ms. Fangqin Guo, Mr. Keita Shinzato, Mr. Hiroyuki Kurihama, Mr. Hironori Kawai, Mr. Chiaying Lu, Prof.

Dr. Jean-Pierre Bonnet and Mr. Keiji Takagishi.

I would like to express my special thanks to Ms. Misao Mukoda and Ms. Saori Inagaki for their support in my doctoral course life.

Finally, without my family, Aki, Kiyomasa and Ruriko, I could not complete my doctoral course. I love you so much.

Research article

Vanadium Hydride as Conversion Type Negative Electrode for All-Solid-State Lithium-ion-battery

Yasuhiro Matsumura, Keiji Takagishi, Hiroki Miyaoka and Takayuki Ichikawa

Materials Transactions 60 (2019) 2183-2187.